CONF-8310198--6

Revised
12-9-83

REVIEW OF MECHANICAL PROPERTIES AND MICROSTRUCTURES OF TYPES 304 AND 316 STAINLESS STEEL AFTER LONG-TERM AGING*

J. A. Horak and V. K. Sikka
Metals and Ceramics Division, Oak Ridge National Laboratory,
Oak Ridge, Tennessee 37831, USA

and

D. T. Raske
Argonne National Laboratory,
Argonne, Illinois 60439

CONF-8310198--6

DE85 000969

ABSTRACT

Because commercial liquid metal fast breeder reactors (LMFBRs) will be designed to last for 35 to 40 years, an understanding of the mechanical behavior of the structural alloys used is required for times of 2.2 to 2.5×10^5 h (assuming a 70% availability factor). Types 304 and 316 stainless steel are used extensively in LMFBR systems. These alloys are in a metastable state when installed and evolve to a more stable state and, therefore, microstructure during plant operation. Correlations of microstructures and mechanical properties during aging under representative LMFBR temperature and loading conditions is desirable from the standpoint of assuring safe, reliable, and economic plant operation. We reviewed the mechanical properties and microstructures of types 304 and 316 stainless steel wrought alloys, welds, and castings after long-term aging in air to 9×10^4 h (about 10-1/2 years). The principal effect of such aging is to reduce fracture toughness (as measured in Charpy impact tests) and tensile ductility. Examples are cited, however, where, because stable microstructures are achieved, these as well as strength-related properties can be expected to remain adequate for service life exposures.

INTRODUCTION

Commercial liquid metal fast breeder reactor (LMFBR) power plants will be designed for lifetimes of 35 to 40 years. For these plants to operate safely, reliably, and economically for their full lifetimes, the major components of the plant must perform satisfactorily for comparable periods of time.

*Research sponsored by the Office of Breeder Technology Projects, Office of Nuclear Energy, U.S. Department of Energy, under contract W-7405-eng-26 with Union Carbide Corporation.

To ensure that a commercial LMFBR plant can meet its design objectives requires the capability to predict the behavior of structural alloys for times of 2.2 to 2.5 × 10^5 h (assuming an availability factor of 70%). For this purpose, correlations between the microstructures and the mechanical properties of these alloys during aging under representative LMFBR temperatures and loading conditions are desirable. Such correlations are useful for extrapolating materials behavior to anticipated design lifetimes, interpolating materials behavior to conditions that are intermediate to those used in laboratory tests, predicting the response of components and structures to off-normal operation conditions, and providing the information necessary to scale up from laboratory test conditions and specimen sizes to full-size reactor components and structures.

Types 304 and 316 stainless steel are the major structural alloys used in LMFBR designs. An example of their application in the Clinch River Breeder Reactor Plant is shown in Fig. 1 (ref. 1). These alloys are in a metastable thermodynamic state at the beginning of plant operation. During prolonged exposure to the temperatures and stresses of LMFBR operation, they evolve to more stable thermodynamic states and, therefore, microstructures. Weiss and Stickler described the thermodynamics and the microstructural changes that occur in type 316 stainless steel when the solid solution austenite is exposed to elevated temperatures for long times.[2]

This paper presents information generated in the U.S. Department of Energy LMFBR Materials and Structures Program on (a) the mechanical properties of types 304 and 316 stainless steel wrought alloys, welds, and castings after long-term aging in air to 9 × 10^4 h (about 10-1/2 years) at temperatures in the range of 427 to 649°C (800 to 1200°F), after creep, and after fatigue deformation and (b) microstructural evolution during long-term aging and testing for these alloys.

REVIEW AND DISCUSSION OF PROPERTIES AND MICROSTRUCTURES

WROUGHT ALLOYS

Tensile Properties

The effects of laboratory aging or service exposure to times of 5.1 × 10^4 h at temperatures to 649°C (1200°F) on the microstructure and tensile properties of mill-annealed type 316 stainless steel are shown in Fig. 2 (ref. 3). In the unaged condition the microstructure shows only high-angle grain boundaries. After 4.4 × 10^3 h (about 6 months) at 649°C (1200°F) (0.53 T_m for this alloy where T_m is the absolute melting temperature), large carbide particles are present on these boundaries. After 5.1 × 10^4 h (about 6 years) at this temperature, carbide precipitation has occurred within the grains as well as at the grain boundaries; carbon, chromium, nickel, and molybdenum originally in solid solution are found in the large particles shown in Fig. 2. The strength properties after aging are within the scatter band of these properties for unaged material.

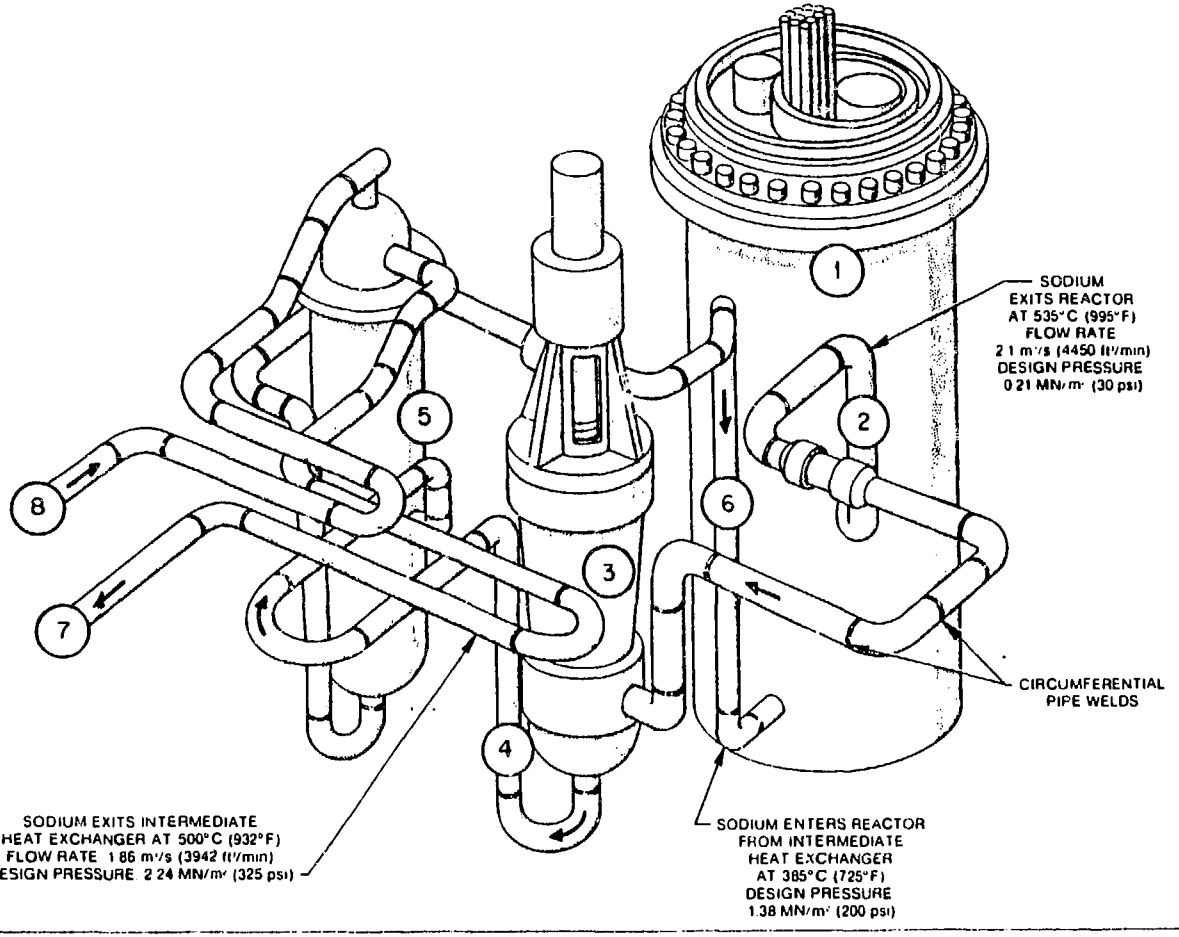

Fig. 1. Uses of types 304 and 316 stainless steel and their weldments for out-of-core structures and components of the Clinch River Breeder Reactor Plant (ref. 1).

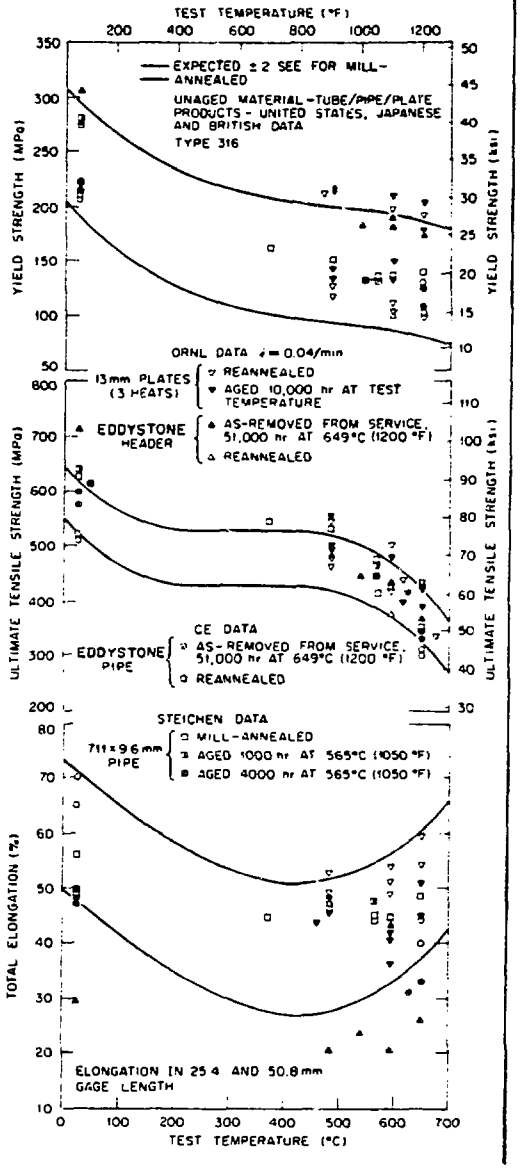

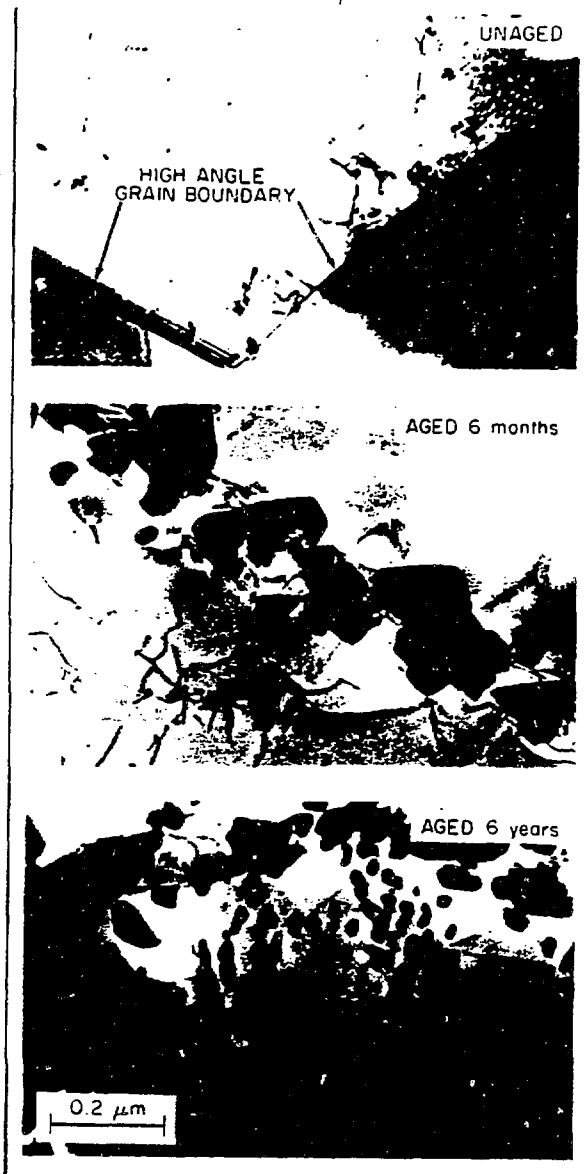

Fig. 2. Tensile properties and microstructures of type 316 stainless steel in the mill annealed, aged for times to 5.1×10^4 h (about 6 years) and reannealed after aging conditions (ref. 3).

Additional information on the effects of longer term aging on the tensile properties of type 316 stainless steel is contained in Figs. 3 and 4. The data in Fig. 2 are for only four aging times, but those in Figs. 3 and 4 are for 12 aging times.[4-10] For the important temperature range of application for this steel in LMFBRs [500–625°C (930–1160°F)], the 0.2% yield and ultimate tensile strengths are either unaffected or increased by aging. Thus, it is reasonable to state that no unforeseen decreases in strength will occur for unstressed material for service times between about 10 1/2 years (Figs. 3 and 4) and the service lifetime of 25 to 28 years for commercial LMFBRs. For some of the times shown in Figs. 3 and 4, at temperatures above 550°C (1022°F) precipitation reactions are essentially complete for this alloy, and a stable matrix and grain-boundary structure should be present. For aging temperatures of 593°C (1100°F) and above the ductility falls below the minimum ductility measured on unaged material. However, total elongation and reduction of area are still above 25%, which is acceptable. Some implications of the lower ductility of aged material are discussed below under "Toughness Properties."

Knowledge of the effects of prior loading also is needed for extrapolation to conditions beyond laboratory tests. Figures 5 and 6 contain data on the effects of prior creep and fatigue loading, respectively, on the tensile properties of type 304 stainless steel.[3,11] At 538 and 593°C (1000 and 1100°F), strength and ductility properties decrease linearly as a function of prior creep strain. Prior creep strain of 0.17 to 0.18 produces a 20% decrease in ultimate tensile strength but a much larger decrease in ductility, as shown by the 50% decrease in total elongation.

Cyclic loading at 593°C (1100°F) and a total strain range of 0.4% has no effect on the tensile properties of type 304 stainless steel at this temperature, even for cycling to 75% of the fatigue life (cycles to failure). For a total strain range of 1.0% the yield strength increases by about 25%, the ductility decreases by about 25%, and the ultimate tensile strength is not affected. Adding tensile hold times of 0.1 and 0.5 h in each cycle at the 1% strain range has no further effect on the yield or ultimate tensile strength, but the ductility decreases with increasing hold time. At 75% of the fatigue life, the ductility decreases almost 50% by a 0.1-h hold time, and at only 50% of the fatigue life the ductility is reduced by a 0.5-h hold time to only 43% of that before the creep-fatigue loading. This information indicates that continuous-cycling fatigue loading at maximum strain ranges to 1% at 593°C (1100°F) has little, if any, effect on the tensile properties of type 304 stainless steel. The data in Fig. 6, combined with the data shown in Fig. 5, illustrate that creep damage produced in either monotonic or cyclic loading is detrimental to tensile properties. The tensile property most affected by creep loading is ductility. Discussion of this decrease in ductility is presented below under "Toughness Properties."

Creep-Rupture Properties

Figure 7 shows the forms of $Cr_{23}C_6$ precipitate particles in type 304 stainless steel after a creep-rupture test lasting 6×10^4 h at 593°C (1100°F) and 117 MPa.[12,13] The precipitate particles are large (50–100 nm across) and primarily rectangular. Figure 8 shows massive precipitates of sigma phase and fine precipitates of $Cr_{23}C_6$ in the same sample. Fig. 9 shows

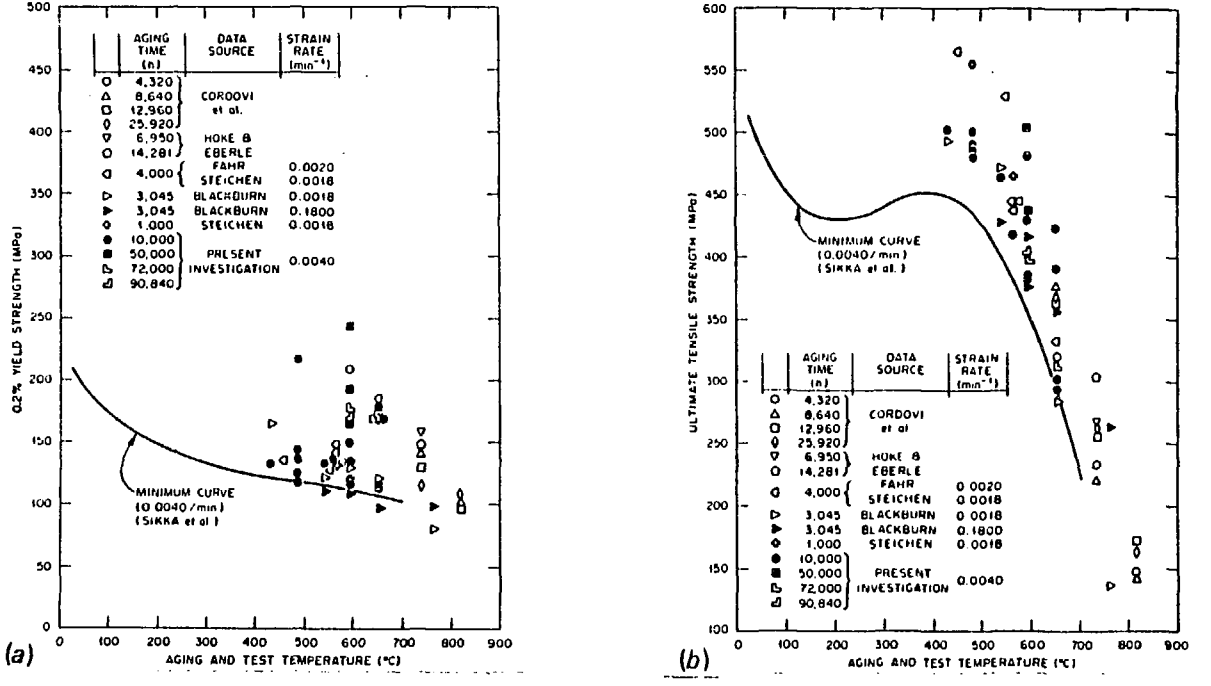

Fig. 3. Yield and ultimate strengths of type 316 stainless steel in the annealed condition and after aging for times to 9.1×10^4 h (about 10 1/2 years) (refs. 4 through 10).

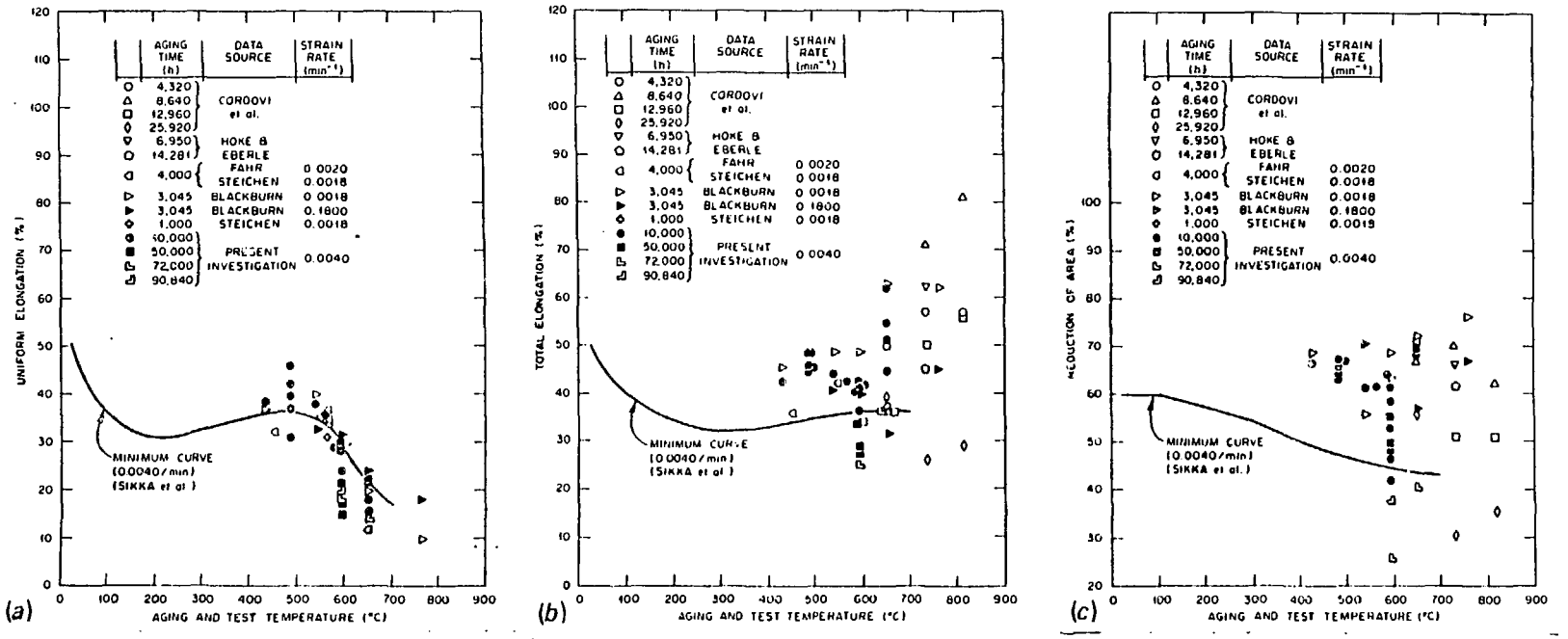

Fig. 4. Uniform and total elongation and reduction of area of type 316 stainless steel in the annealed condition and after aging for times to 9.1×10^4 h (about 10 1/2 years) (refs. 4 through 10).

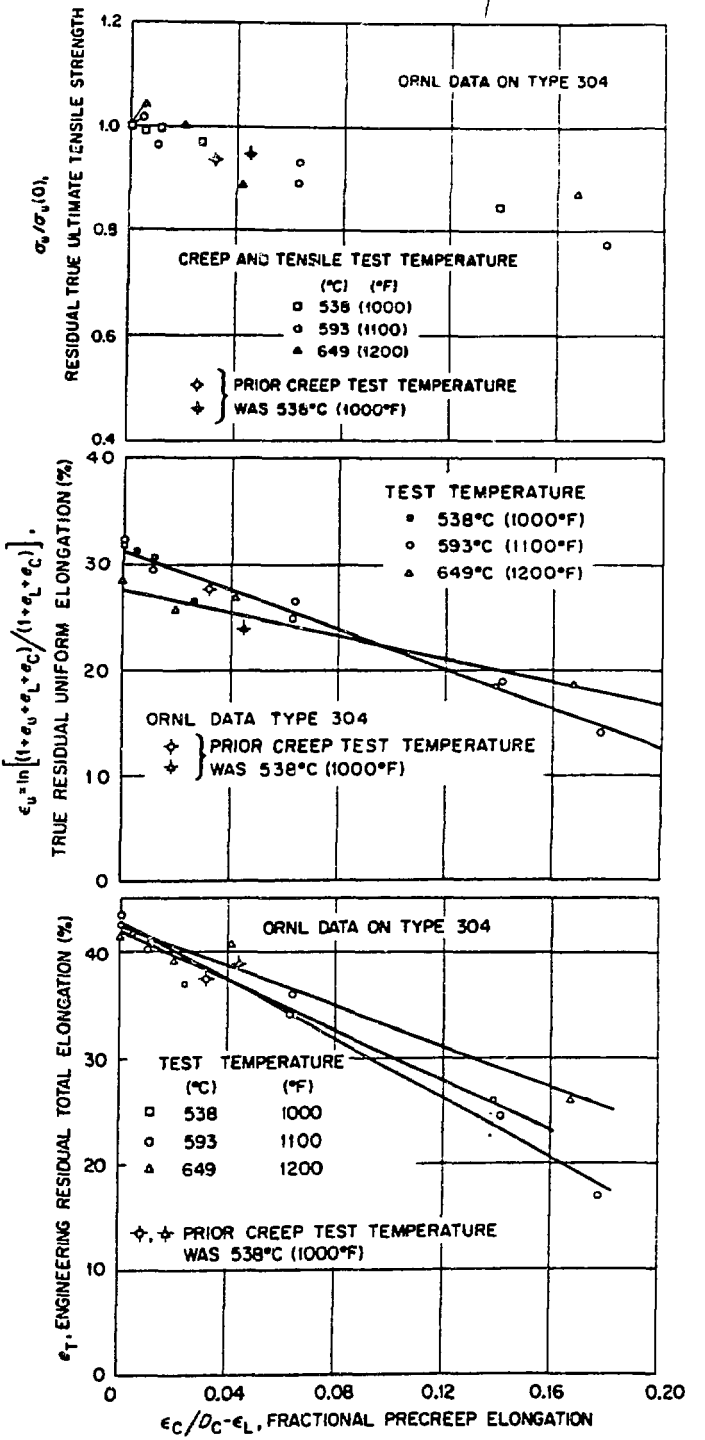

Fig. 5. Residual tensile properties of type 304 stainless steel at 583, 593, and 649°C (1000, 1100, and 1200°F) as a function of prior creep elongation (ref. 3).

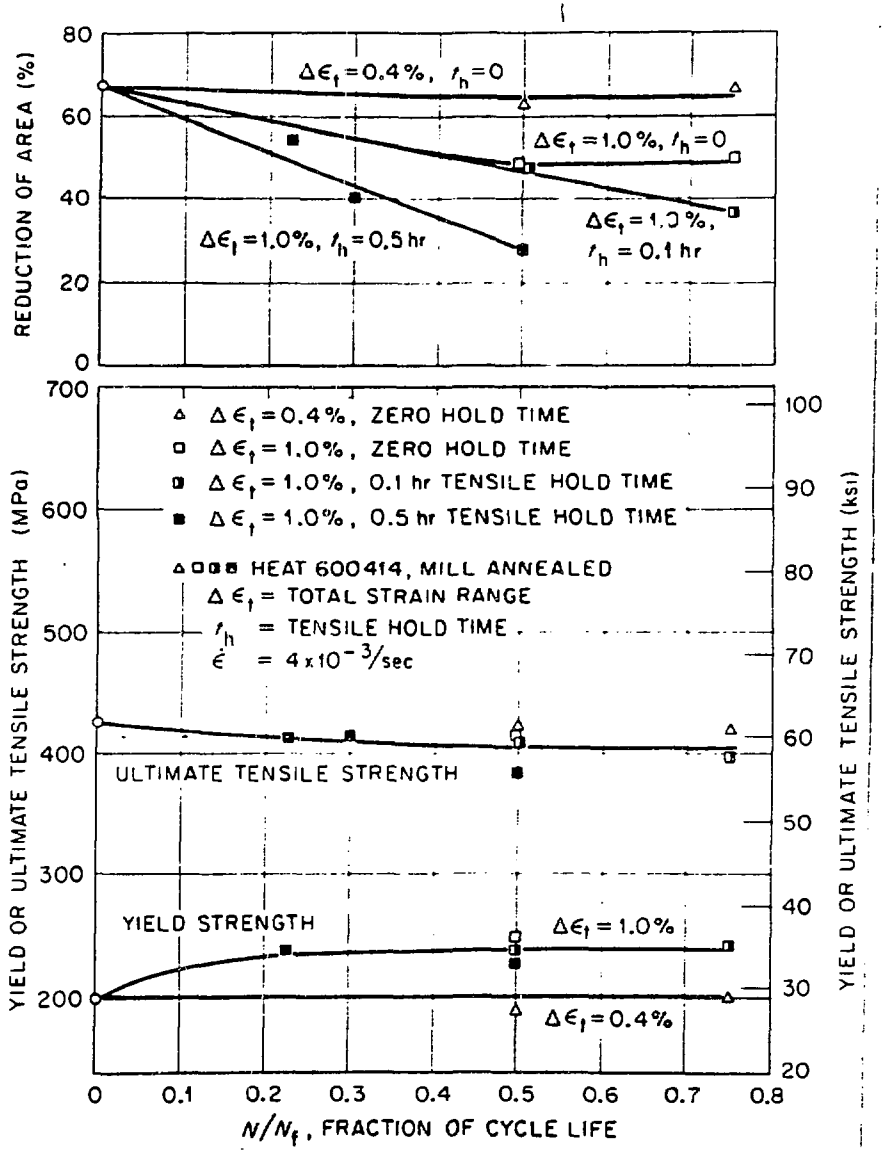

Fig. 6. Tensile properties as a function of cycle life expended for type 304 stainless steel cycled in strain control at 593°C (1100°F) (N_f = cycles to failure) (ref. 11).

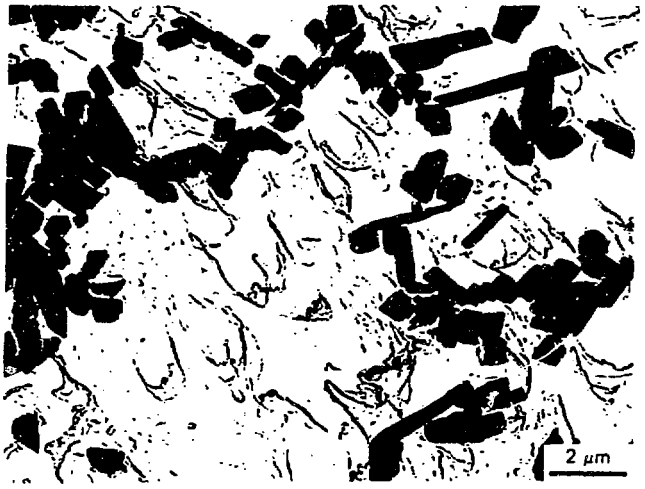

Fig. 7. Transmission electron micrograph of carbon extraction replica showing forms of $Cr_{23}C_6$ particles extracted from the stressed region of type 304 stainless steel after 6×10^4 h (about 7 years) at 593°C (1100°F) and 117 MPa (ref. 13).

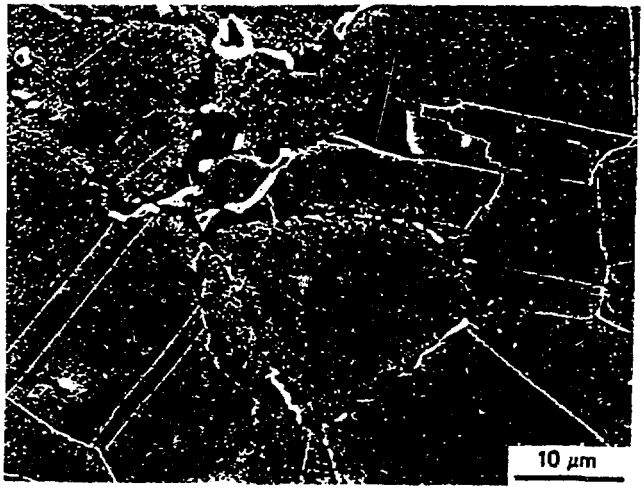

Fig. 8. Scanning electron micrograph showing massive sigma phase and fine particles of $Cr_{23}C_6$ precipitated in the stressed region of type 304 stainless steel during 6×10^4 h (about 7 years) at 593°C (1100°F) and 117 MPa (ref. 13).

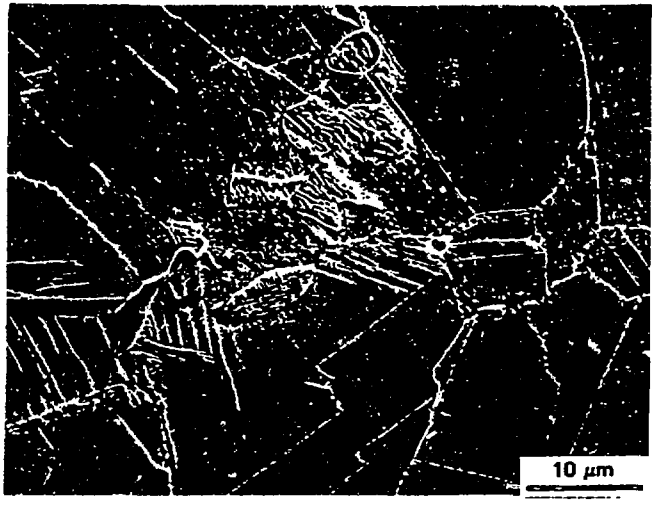

(a)

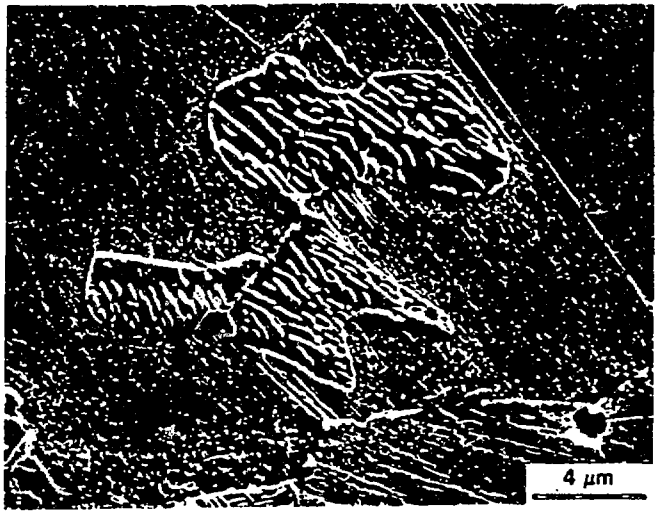

(b)

Fig. 9. Scanning electron micrograph showing large islands of δ-ferrite containing fine particles of sigma phase precipitated in the stressed region of type 304 stainless steel during 6×10^4 h (about 7 years) at 593°C (1100°F) and 117 MPa (ref. 13).

that sufficient localized chromium depletion from the austenite during precipitation of sigma phase can result in the sigma phase particles being surrounded by δ-ferrite.

Figure 10 is an optical micrograph from a creep-rupture specimen of type 304 stainless steel that ruptured after 7.3×10^4 h (about 8 1/2 years) at 593°C (1100°F) and 117 MPa. At the lower center of the micrograph is evidence that the original grain boundary moved during the test. The matrix in this area is apparently void of any precipitates. Apparently they were dissolved during the grain-boundary movement under the applied stress. The grains contain an essentially uniform distribution of carbide particles, and massive sigma phase particles are found at grain-boundary intersections. The microstructures shown in Figs. 7 through 10 are all in excellent agreement with the relatively short-term aging studies of Weiss and Stickler.[2] The information derived from these figures shows that the time-temperature-precipitation diagrams developed by Stickler and Vinckier for type 304 (ref. 14) and by Weiss and Stickler for type 316 stainless steel (ref. 2) can be very effectively used to predict the microstructures and associated mechanical properties of these alloys for long-term testing and service conditions in the operation of LMFBRs.

Figure 11 contains data for the creep-rupture life for 11 heats of type 304 stainless steel tested at 593°C (1100°F) and the minimum time-to-rupture curve as given in ASME Code Case N-47. Except for a few tests at 172 MPa, these results indicate that the long-term creep-rupture properties for type 304 stainless steel are well above the ASME minimum for rupture lives to 9.6×10^4 h (about 11 years).

Figure 12 shows the creep curves at 593°C (1100°F) and a stress of 172 MPa for type 316 stainless steel in the annealed condition and after aging for 10^4 h (about 1 year) at 593°C (1100°F). This aging increases the secondary (steady-state) creep rate, the rupture life, the rupture ductility, and the time to onset of tertiary creep. The effects of a much longer aging time [4.4×10^4 h (about 5 years)] on the creep rupture curves for type 316 stainless steel at 593°C (1100°F) are shown in Fig. 13 for stress of 207 MPa. At 172 MPa (same stress as in Fig. 12) aging for 4.4×10^4 h (about 5 years) results in a large increase in secondary creep rate and a slight increase in ductility and in a slight decrease in the times to the onset of tertiary creep and rupture. For the higher stress of 207 MPa this aging results in a large increase in the secondary creep rate and ductility and in large decreases in the times to onset of tertiary creep and rupture. Note that aging increases creep ductility (low strain rates) but decreases tensile ductility (high strain rates).

Figure 14 shows stress versus time to rupture at 593°C (1100°F) for type 316 stainless steel annealed and after aging for times to 7.4×10^4 h (about 8 1/2 years) at temperatures from 482 to 649°C (900 to 1200°F). Also shown in Fig. 14 is the minimum stress versus time to rupture from ASME Code Case N-47. For all aging histories shown, the time to rupture for aged material exceeds that for the ASME minimum. Hence, long-term thermal exposures (~5 years) at temperatures up to 649°C (1200°F) and stresses too low to drastically alter the precipitation reactions do not shorten the subsequent creep-rupture life of type 316 stainless steel at temperatures to 593°C (1100°F). As stated for the tensile properties, little or no further effects of aging on the creep-rupture properties are expected as a result of additional thermal exposures at low stresses for temperatures to about 593°C (1100°F).[15]

Fig. 10. Optical micrograph showing large amounts of carbide precipitation within the matrix and large sigma phase particles at the grain boundaries in the stressed region of type 304 stainless steel during 7.3×10^4 h (about 8 1/2 years) at 593°C (1100°F) and 117 MPa.

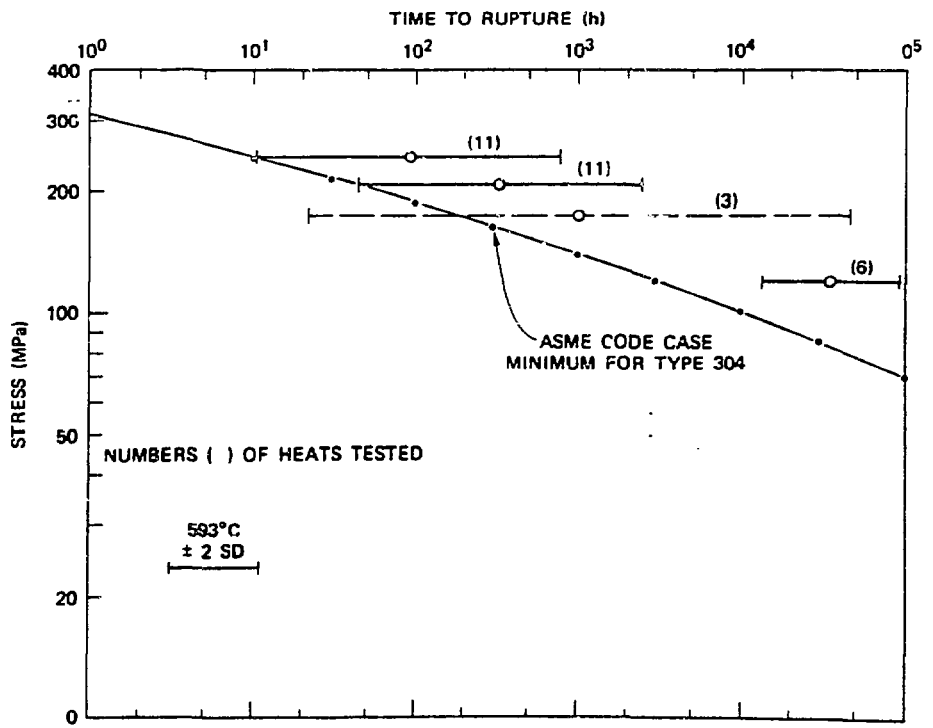

Fig. 11. Stress-rupture properties at 593°C for 11 heats of type 304 stainless steel and ASME Code Case N-47 minimum for type 304 stainless steel at 593°C (1100°F).

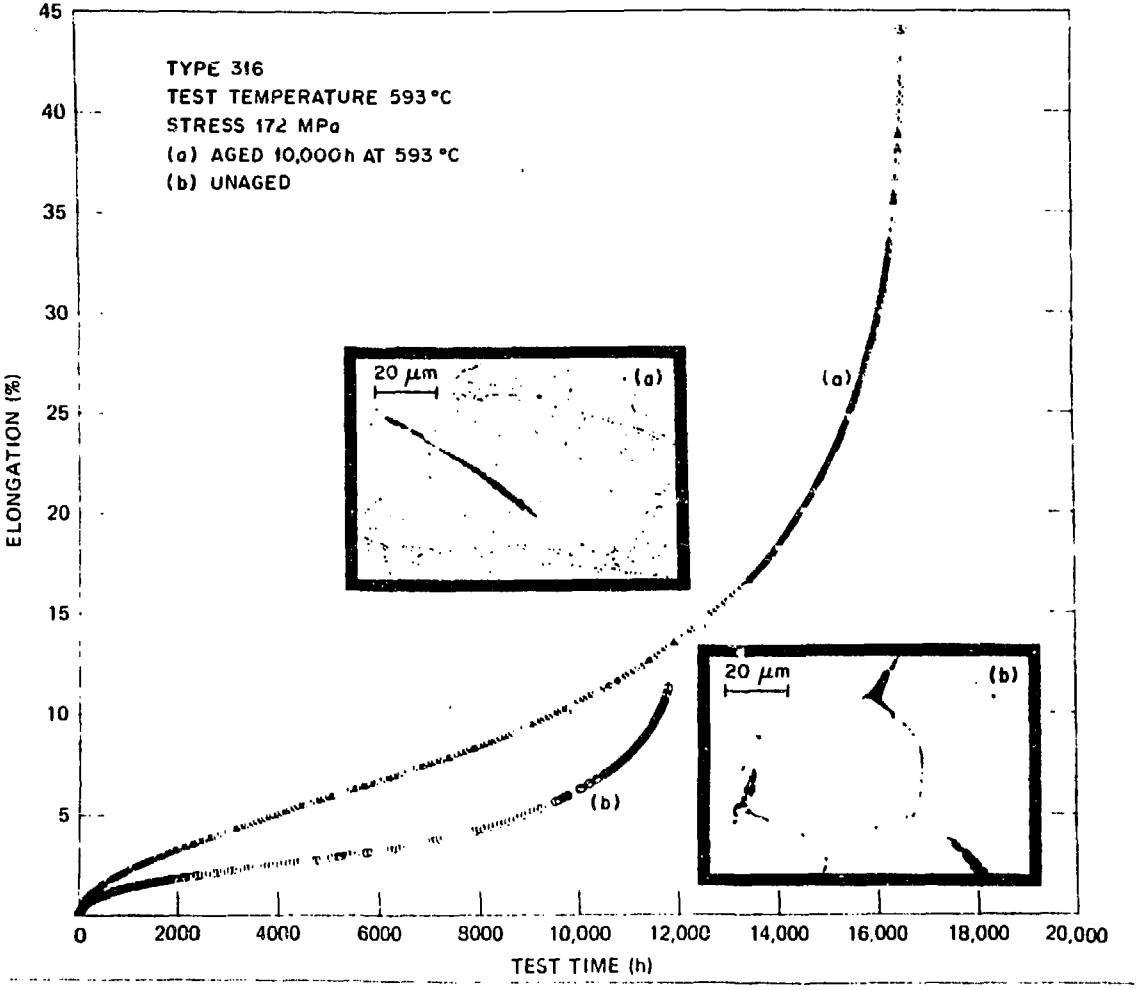

Fig. 12. Elongation as a function of test time at 593°C (1100°F) and 172 MPa and optical microstructures for type 316 stainless steel annealed and after aging for 10^4 h (about 1 year). The micrographs show (*a*) fine precipitate structure, intragranular deformation, and annealing twin cracks in aged material and (*b*) lack of grain deformation and intergranular cracks in annealed material.

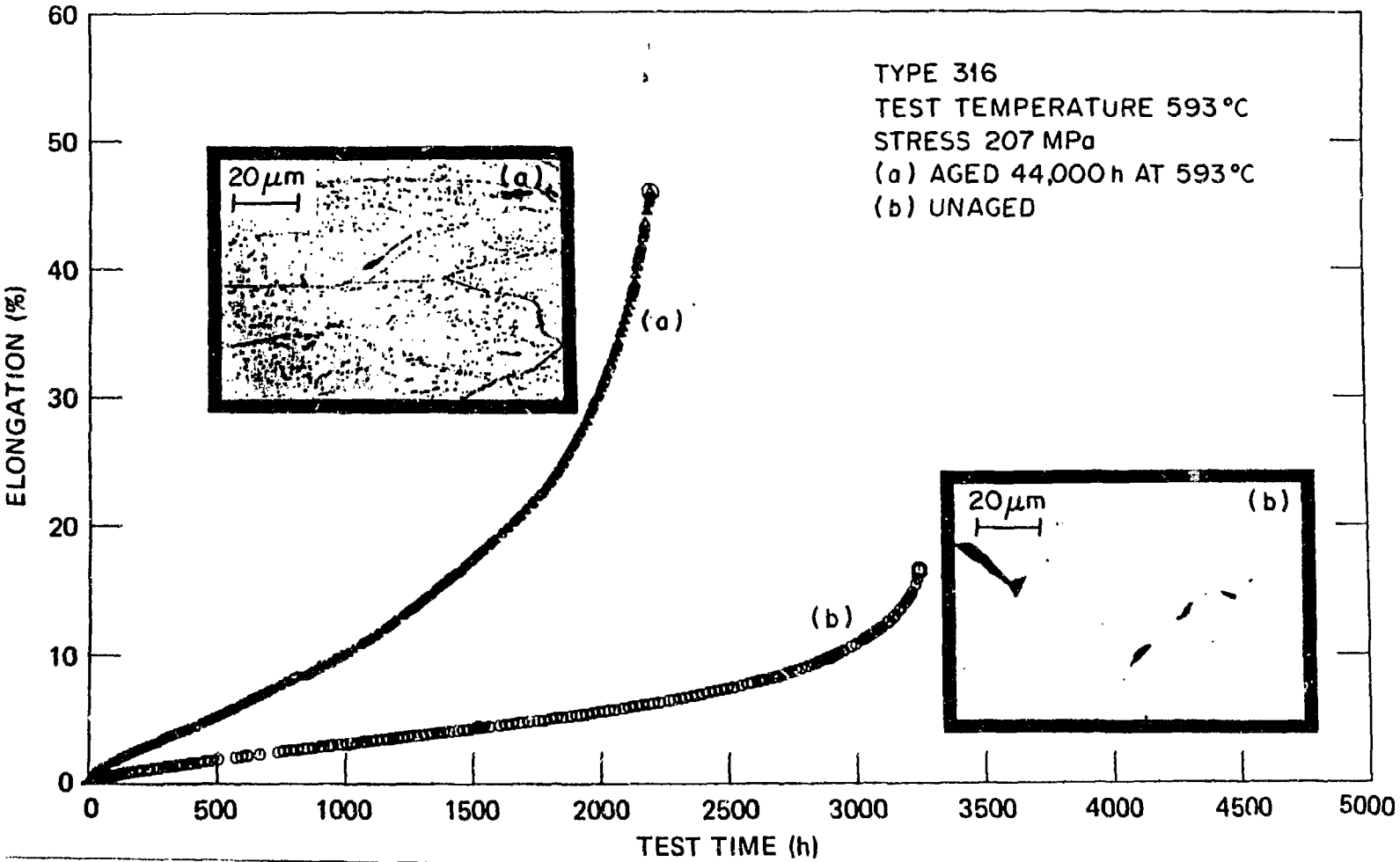

Fig. 13. Elongation as a function of test time at 593°C (1100°F) and 207 MPa and optical microstructures for type 316 stainless steel annealed and after aging for 4.4×10^4 h (about 5 years).

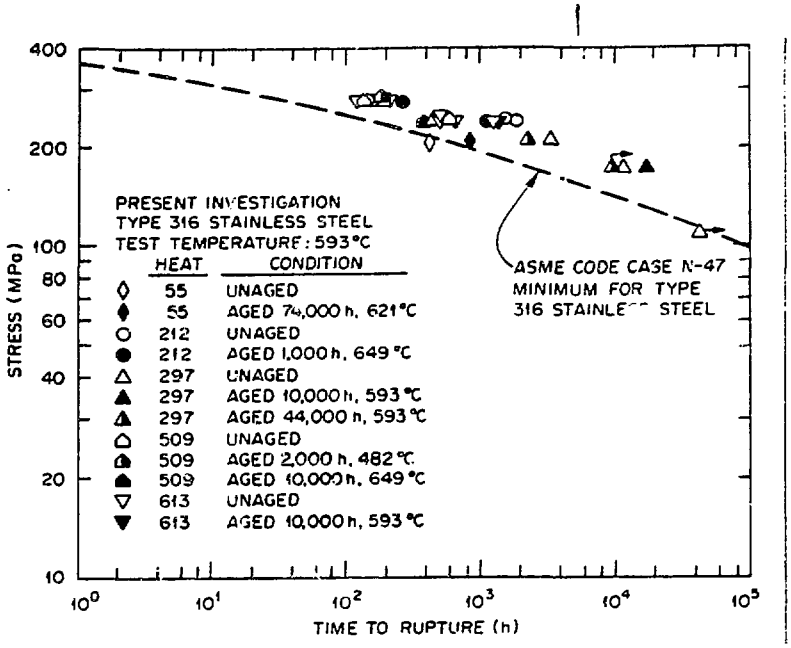

Fig. 14. Stress-rupture properties at 593°C (1100°F) for type 316 stainless steel annealed and after aging to 7.4×10^4 h (about 8 1/2 years) and ASME Code Case N-47 minimum for type 316 stainless steel at 593°C (1100°F).

Figures 15 and 12 show optical metallography for type 316 stainless steel as annealed after aging for 10^4 h (about 1 year) at 593°C (1100°F), and after creep-rupture testing at 172 MPa at 593°C (1100°F). In annealed material the applied stress results in considerable grain-boundary cavitation [Fig. 15(*a*)] and intergranular failure with little or no plastic deformation of the grains, but in aged material the same applied stress results in extensive plastic deformation of the grains and small ductile intragranular cavitation, leading to ductile tearing with no observable grain-boundary cavitation or intergranular failure [Fig. 15(*b*)]. The higher ductility and the associated benefits of the aged material compared with those of the annealed material are clearly evident in Fig. 15. Figure 12, which includes optical micrographs at a much higher magnification than those shown in Fig. 15, shows the details of the microstructure and mode of failure for the aged [Fig. 12(*a*)] and the annealed [Fig. 12(*b*)] materials. The annealed material has some precipitate particles at the grain boundaries but none within the grains. Intergranular cavitation and cracking are the dominant modes of failure. The aged material has many small precipitate particles at the grain boundaries and within the grains. For this microstructure, deformation of grains and nucleation of cracks at annealing twins are the dominant mode of deformation and failure.[16] Precipitation during aging has strengthened the grain boundaries relative to annealed material and has thereby eliminated intergranular cavitation and fracture, resulting in longer creep-rupture life.

Fig. 15. Fracture behavior of type 316 stainless steel creep-rupture tested at 593°C (1100°F) and 172 MPa. (*a*) Annealed; extensive intergranular cracking with large cavities and no intragranular deformation. (*b*) Aged for 10^4 h (about 1 year) at 593°C (1100°F); considerable intragranular deformation with few small to medium-size cavities.

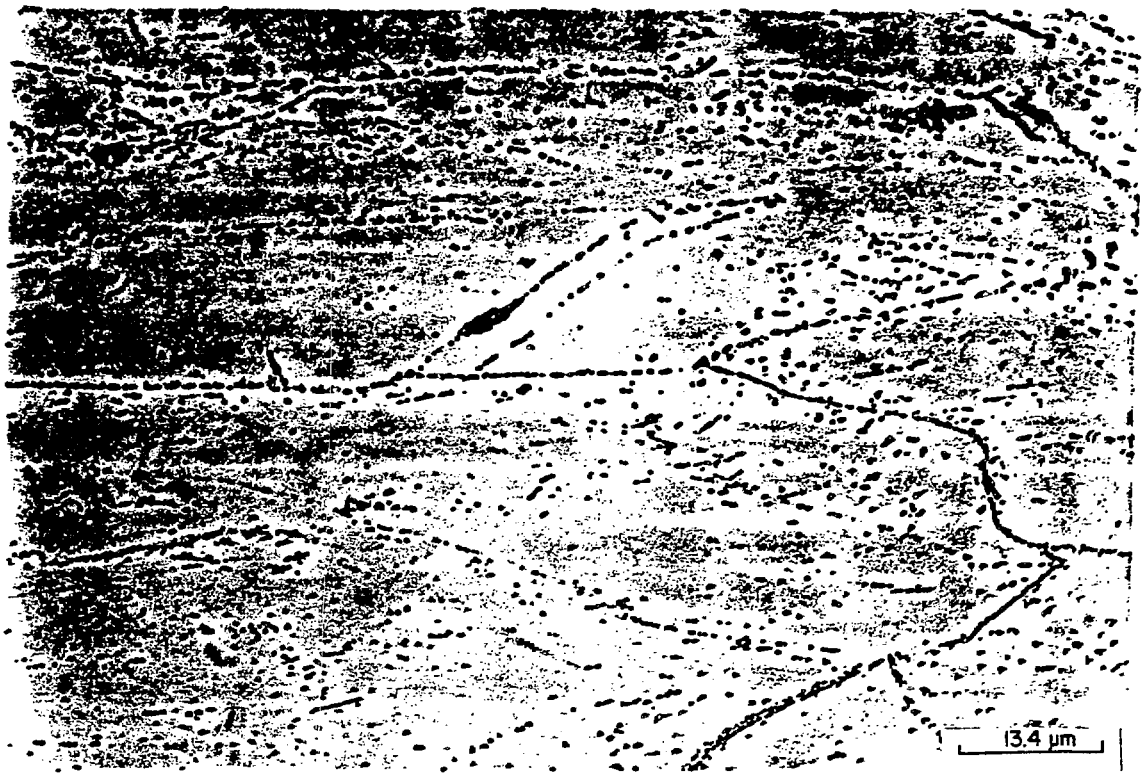

Fig. 16. Optical micrograph of type 316 stainless steel aged for 4.4×10^4 h (about 5 years) at 593°C (1100°F) before creep testing. Precipitate structure and mode of failure are the same as for material aged for 10^4 h (about 1 year) at 593°C (1100°F) shown in Fig. 12.

Figure 16 provides similar information for this alloy aged 4.4×10^4 h at 593°C and creep-rupture tested at 593°C (1100°F) and 207 MPa. The most important aspects of Fig. 16 are that the precipitate structure and deformation mode in the aged material have not changed from that shown in Fig. 12(*a*) for material aged for 10^4 h (about 1 year) before testing at a slightly lower stress. This provides further evidence that the aged structure is stable for elevated-temperature applications in LMFBRs.

Figure 17 shows the sigma phase precipitate present in type 316 stainless steel after 1.25×10^5 h (about 14 1/2 years) of service at 621°C (1150°F) and is very consistent with the analysis of Weiss and Stickler.[2] Although this temperature is well above that anticipated for type 316 stainless steel for out-of-core applications, testing at lower temperatures must be continued to determine if similar structures will be produced by longer exposures at lower temperatures combined with LMFBR operating stresses.

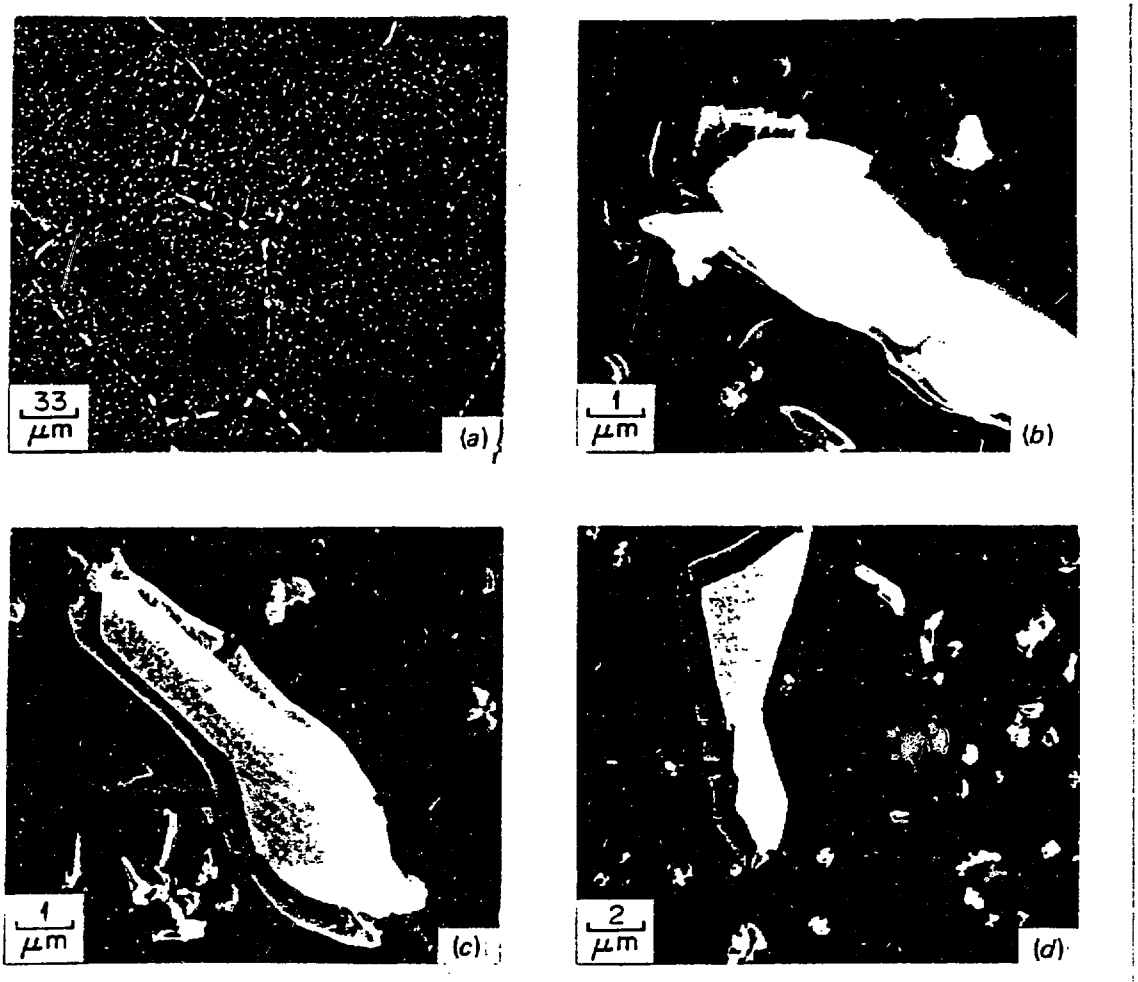

Fig. 17. Scanning electron micrographs of type 316 stainless steel pipe after 1.25×10^5 h (about 14 1/2 years) of service at 621°C (1150°F). (*a*) Overview. (*b*) Laminated structure of large sigma phase particles in the grain boundaries of (*a*). (*c*) Delamination of sigma phase particles and matrix precipitate. (*d*) Delamination of another sigma phase particle and additional matrix precipitate (ref. 12).

Fatigue and Creep-Fatigue Properties

Figures 18 through 20 show the effects of relatively short term aging on the cyclic creep-fatigue lifetimes and microstructures of type 316 stainless steel at 550°C (1022°F). All three figures show the same plots of strain range against fatigue life; however, each of these figures shows a different and important aspect of the microstructures associated with the different fatigue curves. The dashed curve is for continuous cycling. For annealed material (curve *a*) a tensile hold period of 0.5 h during each cycle reduces the creep-fatigue life to only one-fourth that for continuous cycling. Aging for 10^3 h (about 1 month) at 593°C (1100°F) (curve *b*) improves the creep-fatigue life to approximately two-thirds of that for continuous cycling. Aging for 2×10^3 h (about 3 months) at 750°C (1382°F)

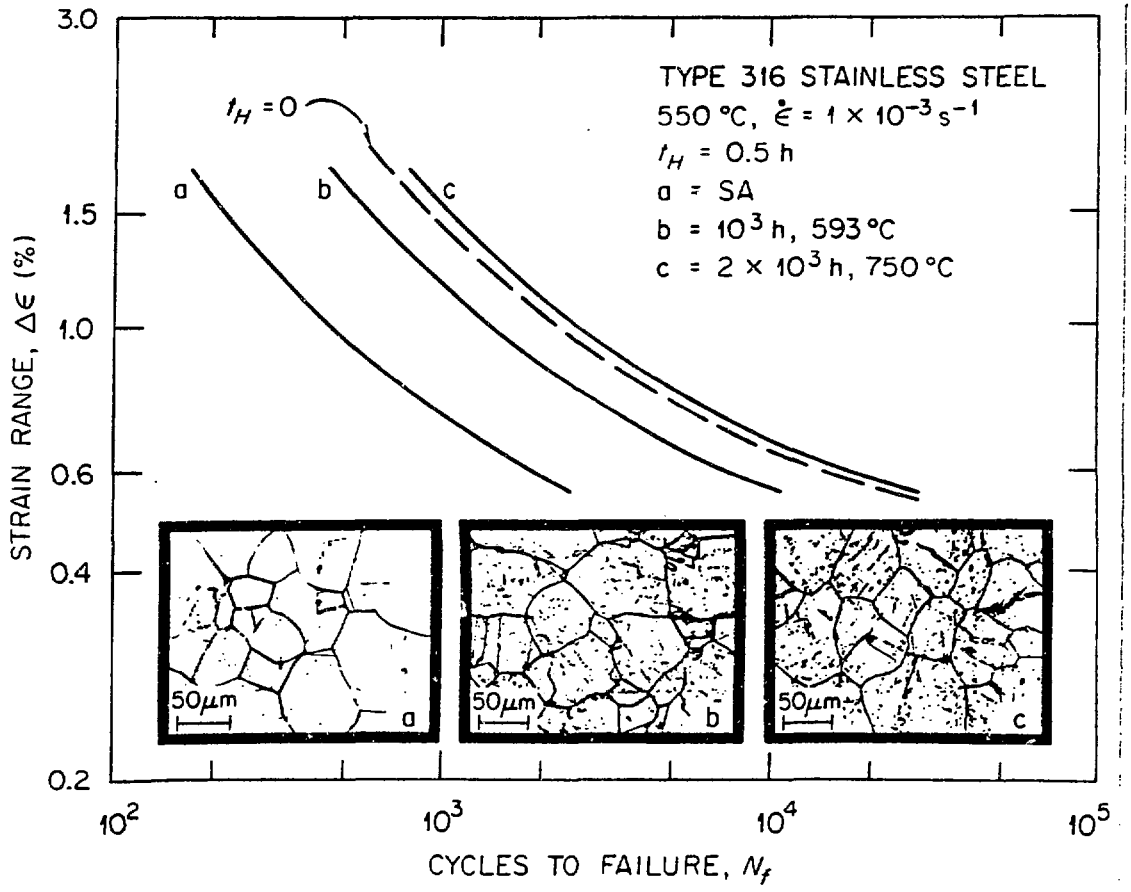

Fig. 18. Strain range versus cycles to failure for cyclic creep-fatigue of type 316 stainless steel at 550°C (1022°F) and optical micrographs for material (*a*) as annealed, (*b*) aged for 10^3 h (about 1 month) at 593°C (1100°F) and, (*c*) aged for 2×10^3 h (about 3 months) at 750°C (1382°F). Dashed line is for continuous cycling fatigue with no hold time.

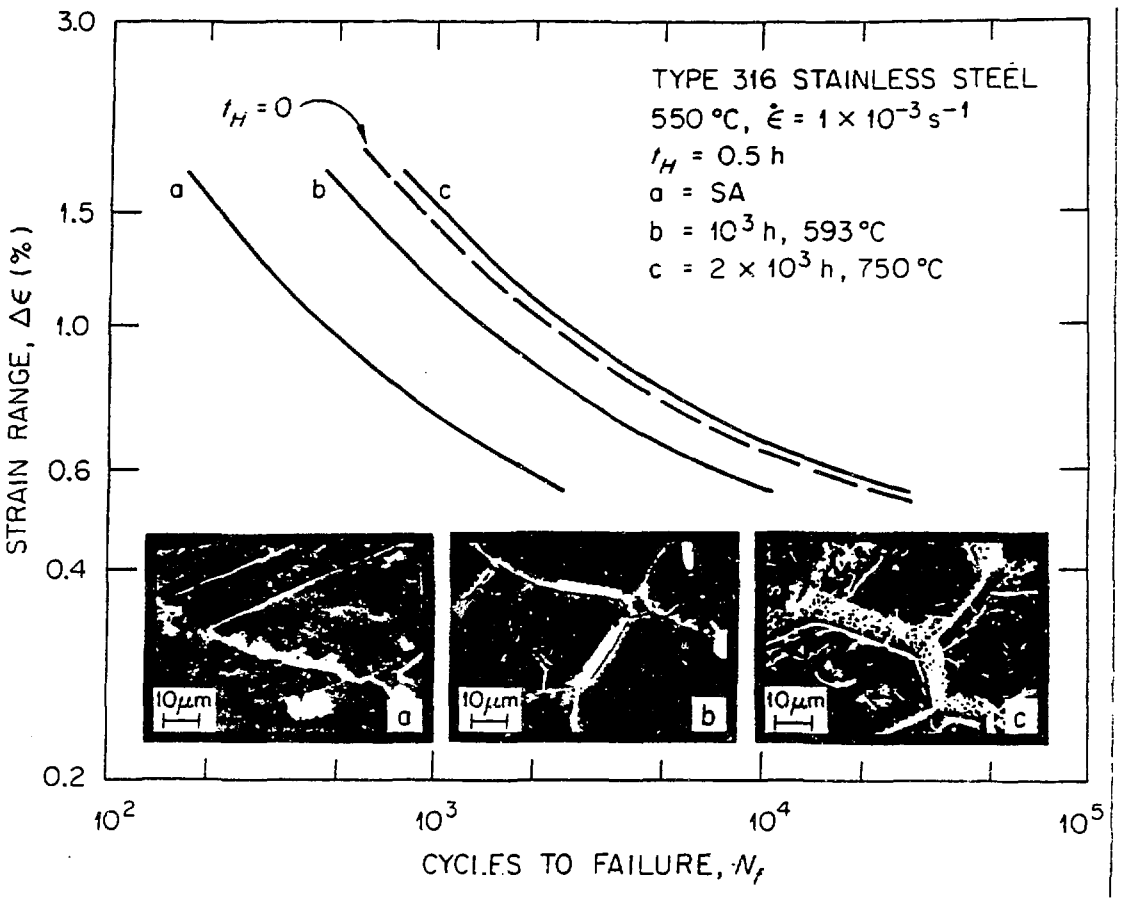

Fig. 19. Strain range as a function of cycles to failure for cyclic creep-fatigue of type 316 stainless steel at 550°C (1022°F) and scanning electron micrographs for material (*a*) as annealed, (*b*) aged for 10^3 h (about 1 month) at 593°C (1100°F), and (*c*) aged for 2×10^3 h (about 3 months) at 750°C (1382°F). Dashed line is for continuous cycling fatigue with no hold time.

(curve *c*) improves the creep-fatigue life to almost 25% greater than that for continuous cycling and more than 4 times that for unaged material under the same test conditions. Aging also improves the continuous-cycling fatigue life, but the magnitude of the improvement is not as great as that for the creep-fatigue life.

The microstructure is shown by optical microscopy in Fig. 18. The annealed material (*a*) shows a small amount of precipitation ($M_{23}C_6$) at the grain boundaries and very little observable precipitation within the grains. In (*b*) more precipitation occurs at the grain boundaries, and precipitation is observable at annealing twin boundaries and other sites within the grains. In (*c*) more massive precipitation is seen at the grain

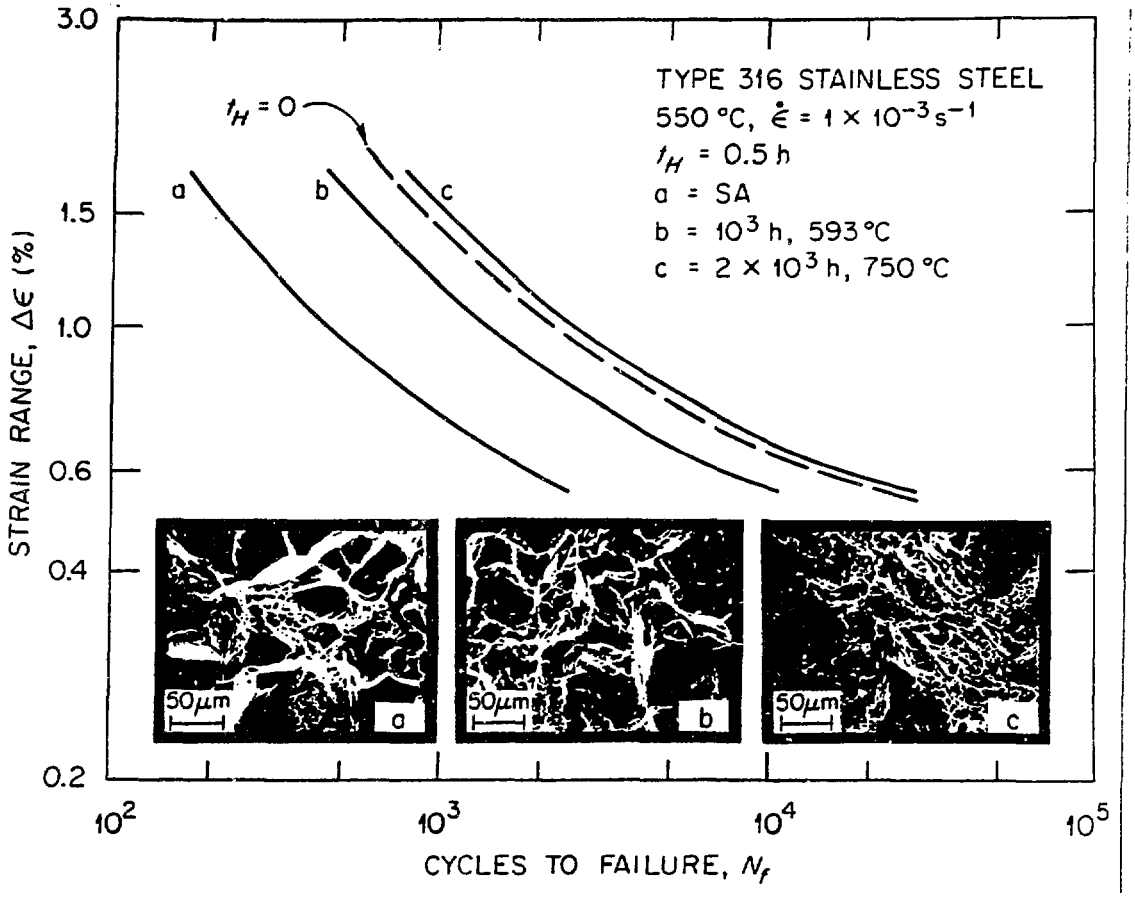

Fig. 20. Strain range versus cycles to failure for cyclic creep-fatigue of type 316 stainless steel at 550°C (1022°F) and scanning electron fractographs for material (*a*) as annealed, (*b*) aged for 10^3 h (about 1 month) at 593°C (1000°F), and (*c*) aged for 2×10^3 h (about 3 months) at 750°C (1382°F). Dashed line is for continuous cycling fatigue with no hold time.

boundaries and within the grains, and the intragranular precipitate particles appear to be larger than in (*b*). Figure 19 shows scanning electron microscopy for material having the creep-fatigue lives shown by curves *a*, *b*, and *c*. The amount of grain-boundary precipitate increases by large increments during aging, as shown in micrographs (*a*), (*b*), and (*c*). This figure clearly shows that the increase in creep-fatigue life on aging is due to the alteration of the grain-boundary and matrix structure by the precipitation.

Figure 20 shows scanning electron fractography associated with creep-fatigue curves (*a*), (*b*), and (*c*). For annealed material (*a*) fracture is intergranular with very little evidence of ductile behavior. For (*b*) intergranular failure is combined with some ductile tearing. In (*c*) the fractograph indicates that failure was totally by intragranular ductile

tearing, with no evidence of brittle intergranular failure. As discussed earlier, alteration of the grain-boundary and matrix microstructure by these precipitates reduces or eliminates grain-boundary cavitation and cracking during creep loading and thereby improves the creep-rupture and creep-fatigue properties.

Toughness Properties

The Charpy impact properties of austenitic stainless steels are not measured or cited very often because austenitic stainless steels normally do not lose fracture toughness or change from ductile to brittle behavior at low temperatures. However, as shown in Fig. 21(*a*), prolonged elevated-temperature exposure of type 316 stainless steel can result in room-temperature Charpy impact energies that are less than 10% of that for material in the annealed and unaged condition. Data in Fig. 21(*a*) are for both laboratory test specimens and material taken from actual power plant components.

Recall that, as shown in Figs. 2 through 6, tensile ductility is the property that is affected most by prior creep or fatigue loading or by thermal exposure for type 316 stainless steel. This decrease in tensile ductility is further manifested in the Charpy impact energy values. Charpy impact energy values for type 316 stainless steel weldments with type 16-8-2 weld alloy agree reasonably well with those for base metal, as shown in Fig. 21(*b*). For the time, temperature, and stress conditions shown in Fig. 21(*b*), the Charpy impact properties of the weld metals are superior to those of the base metal.

Work is in progress to attempt to relate the room-temperature Charpy impact properties with the elevated-temperature slower strain rate properties of these materials. This is not considered to be a concern for LMFBR systems because room-temperature Charpy impact values exaggerate the decrease in elevated-temperature toughness on aging and because during operation LMFBR systems are not exposed to temperatures below about 205°C (400°F) (i.e., during refueling).

WELDS

The development of austenitic stainless steel welds with improved mechanical properties has been an objective of LMFBR base technology programs. ASME Code Case N-47 imposes a strain limitation for all structures that operate at temperatures so high that creep can occur. Strain accumulation in the weld is restricted to one-half that in the base metal. In an attempt to increase the strain limits in welded structures of austenitic stainless steels, the role of trace elements on the mechanical properties of types 308, 316, and 16-8-2 stainless steel welds was studied. Boron, phosphorus, and titanium each improve the elevated-temperature mechanical properties of these welds; however, maximum improvement in properties occurs when these welds contain small concentrations of all three of these elements.[18-20] Welds containing controlled concentrations of these elements are referred to as controlled residual element (CRE) welds. The composition that is currently used is 0.002 to 0.008 wt % B, 0.03 to 0.05 wt % P, and 0.35 to 0.80 wt % Ti.[18-20]

Figure 22 shows the improvement in creep rupture life for types 308, 316, and 16-8-2 CRE stainless steel welds relative to the standard alloys. For all tests, the rupture lives of CRE welds exceed those of the standard

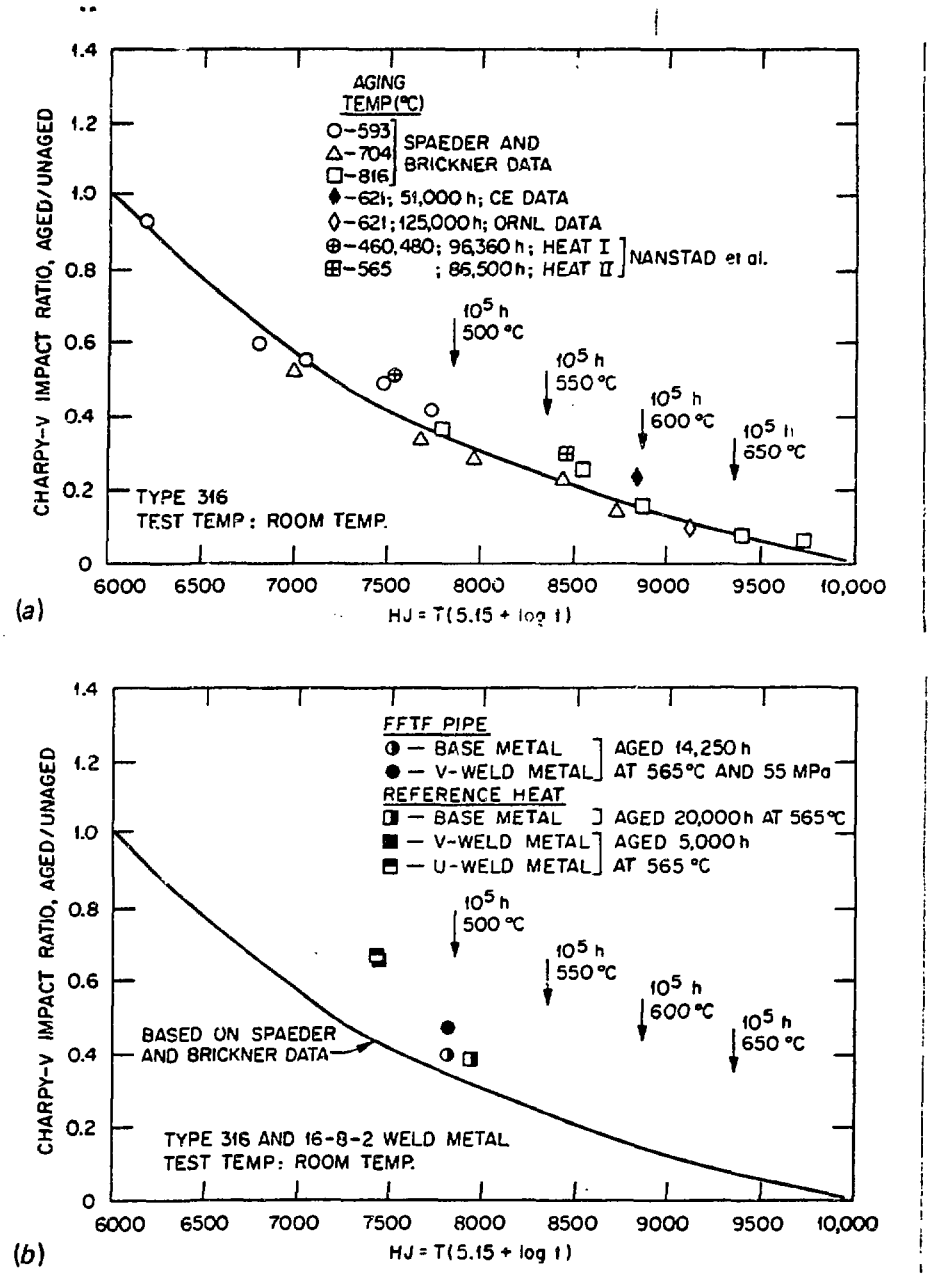

Fig. 21. Room-temperature Charpy impact strength as a function of Holloman-Jaffe parameter for (*a*) type 316 stainless steel after thermal aging or in-service exposure and (*b*) 16-8-2 weld metal after aging for up to 2×10^4 h (2 1/4 years) at 565°C (1050°F). (Ref. 7 and unpublished data from tests performed by ORNL and by Combustion Engineering, Inc.)

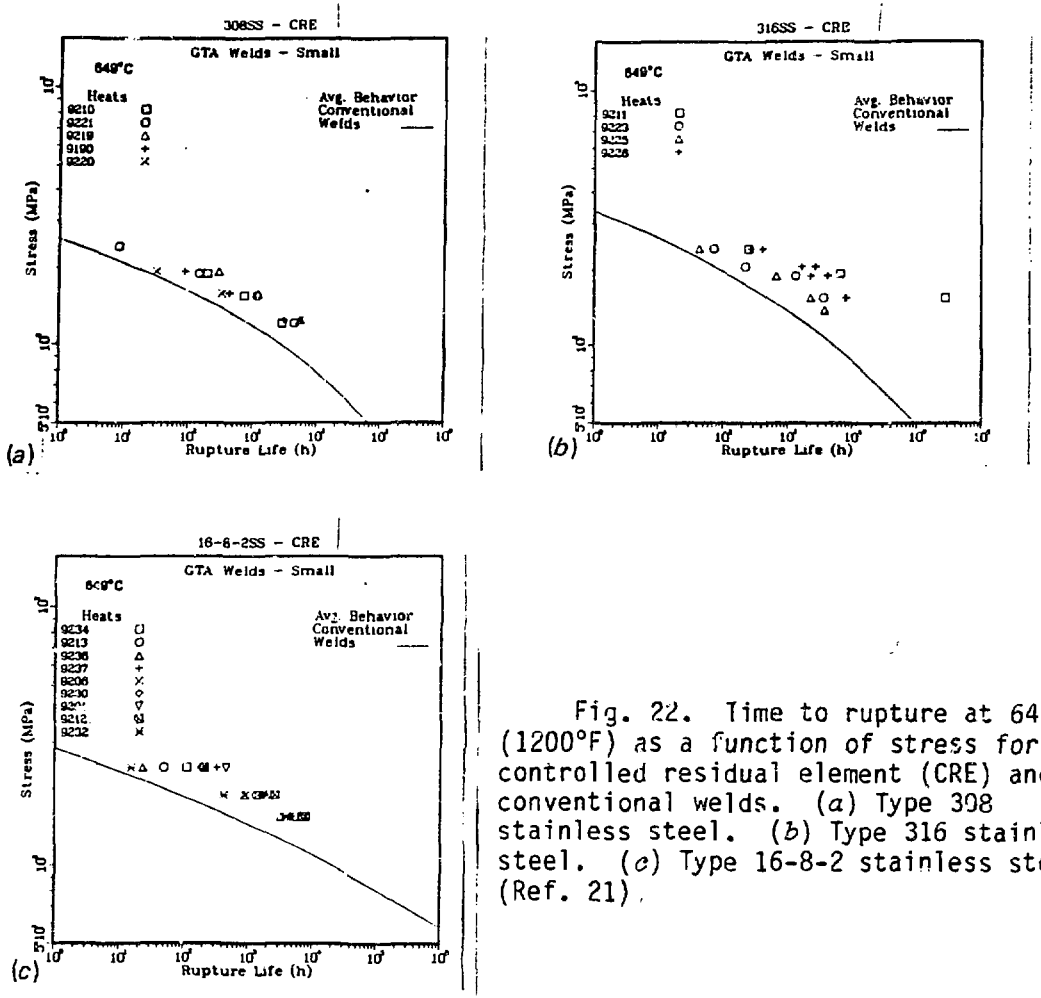

Fig. 22. Time to rupture at 649°C (1200°F) as a function of stress for controlled residual element (CRE) and conventional welds. (*a*) Type 308 stainless steel. (*b*) Type 316 stainless steel. (*c*) Type 16-8-2 stainless steel. (Ref. 21).

alloy. Figure 23 shows that the addition of CRE provides a significant improvement in rupture life at 649°C (1200°F) for 16-8-2 weld metals. Also shown in Fig. 23 are microstructures of (*a*) gas tungsten arc (GTA) type 16-8-2 CRE welds and (*b*) GTA type 16-8-2 standard commercial welds. The microstructure of the CRE weld is much more uniform and on a much finer scale than that for the standard commercial weld metal. Figure 24 shows the microstructure of (*a*) CRE and (*b*) commercial 16-8-2 welds tested under the same conditions. The standard weld has a coarse dendritic microstructure with extensive cracking predominantly at the interfaces between austenite and δ-ferrite. The microstructure in the CRE weld is much finer and free of cracks.

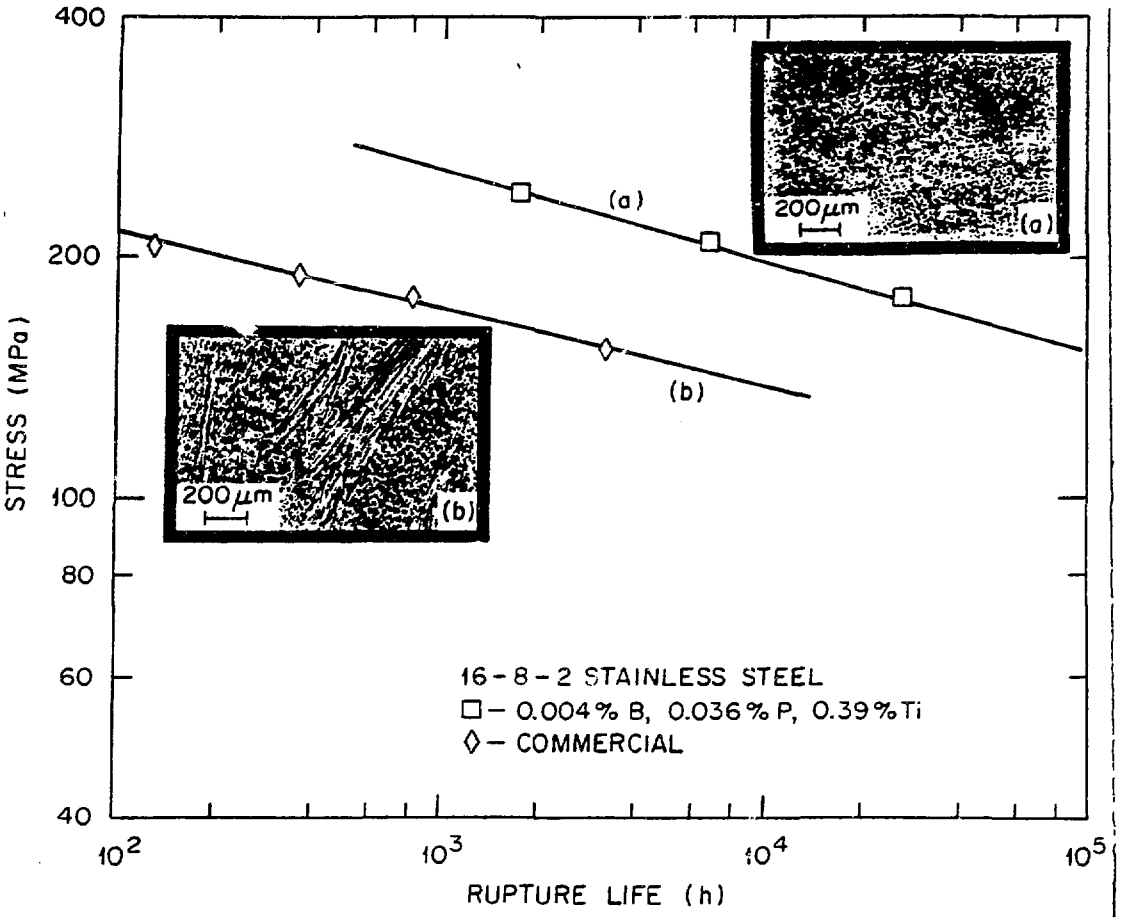

Fig. 23. Stress-rupture properties at 649°C (1200°F) and associated optical microstructures for commercial and controlled residual element (CRE) gas tungsten arc type 16-8-2 welds.

Figure 25 shows the minimum rupture life versus applied stress for GTA and submerged arc (SA) CRE welds and standard welds as calculated by the ASME procedure for base metals. In all three cases, the CRE welds are superior. Figure 26 shows the ASME Code Case N-47 stress-rupture reduction factors for commercial 16-8-2 welds at 454, 538, and 593°C (850, 1000, and 1100°F) and the proposed stress-rupture reduction factor for 16-8-2 CRE welds for temperatures to 593°C (1100°F). For CRE welds no reduction from unity is required for times to 2×10^4 h (about 2 1/4 years), and tests are under way to extend this to times of 10^5 h (about 11 1/2 years) and beyond. These data represent a valuable and significant contribution to the development of austenitic stainless steel filler metals and weldments with improved mechanical properties.

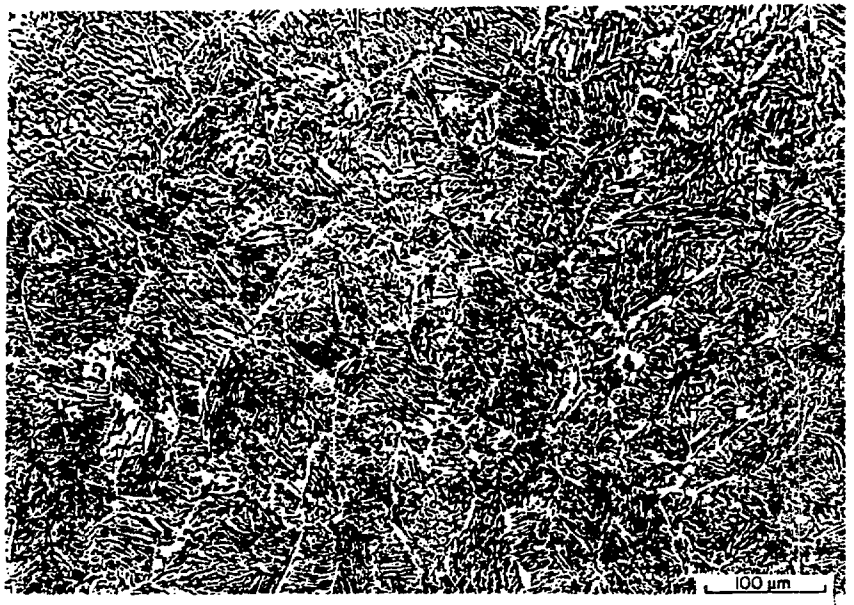

(a)

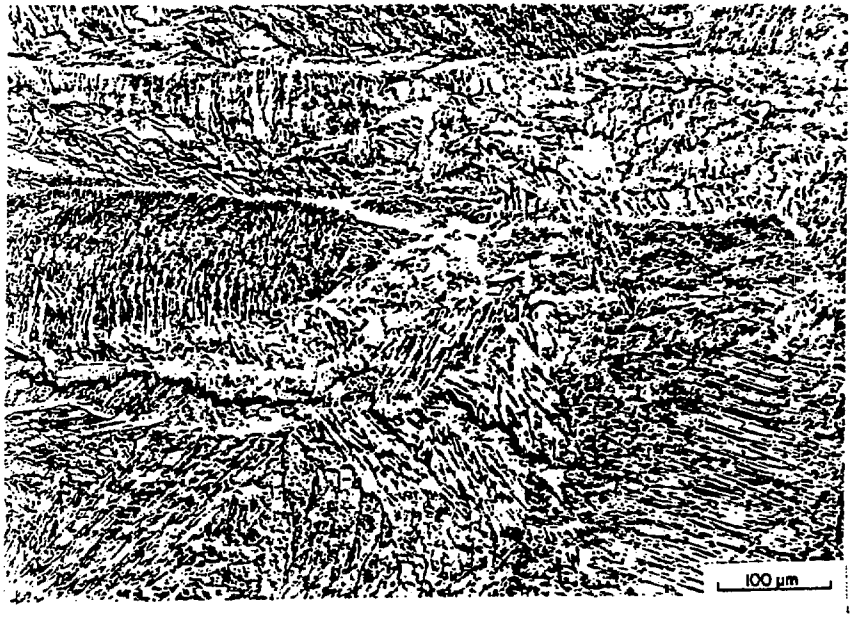

(b)

Fig. 24. Optical micrographs showing (*a*) fine equiaxed structure of controlled residual element (CRE) 16-8-2 welds and (*b*) coarse anisotropic structure with extensive cracking of a commercial 16-8-2 weld.

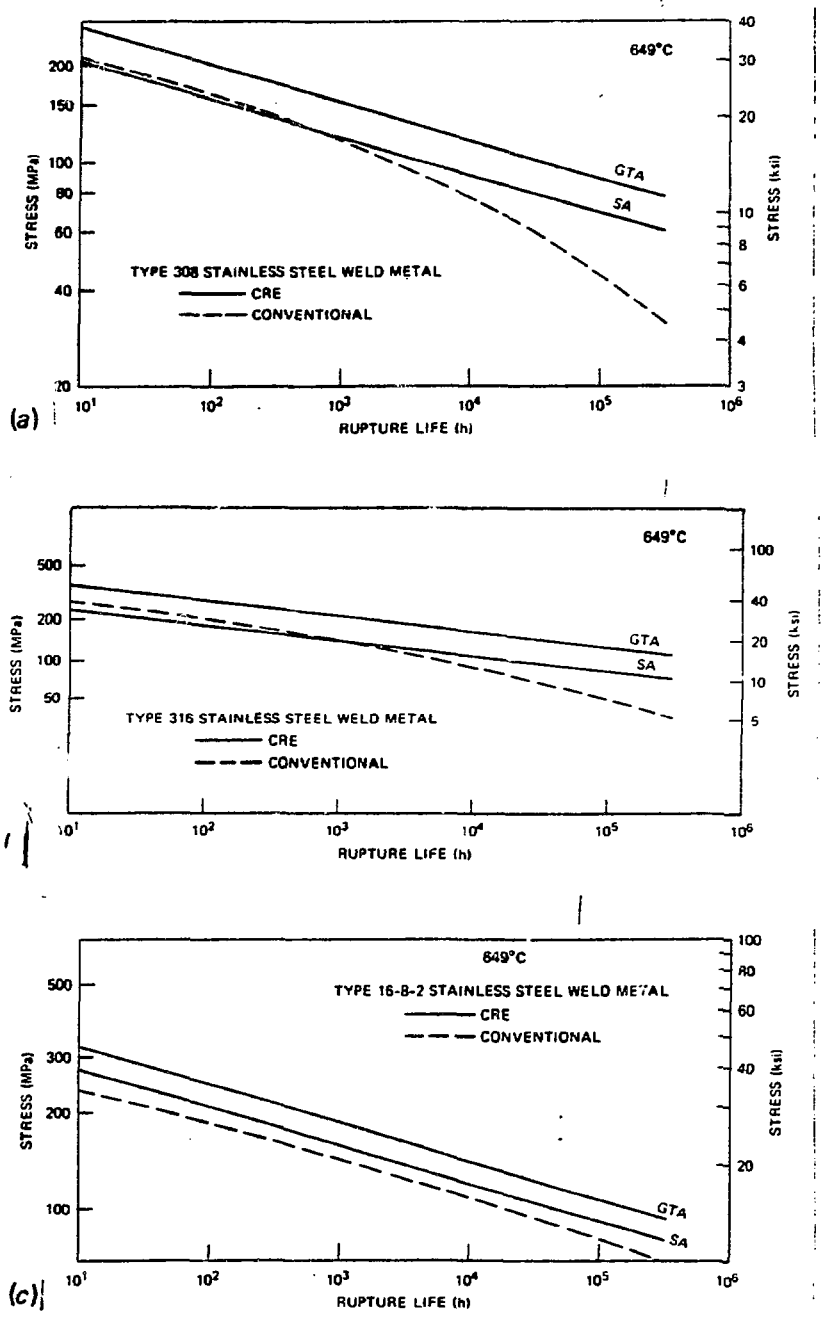

Fig. 25. Time to rupture as a function of applied stress at 649°C (1200°F) for conventional and controlled residual element (CRE) submerged arc (SA) and gas tungsten arc (GTA) welds. (*a*) Type 308 stainless steel. (*b*) Type 316 stainless steel. (*c*) Type 16-8-2 stainless steel. (Ref. 21).

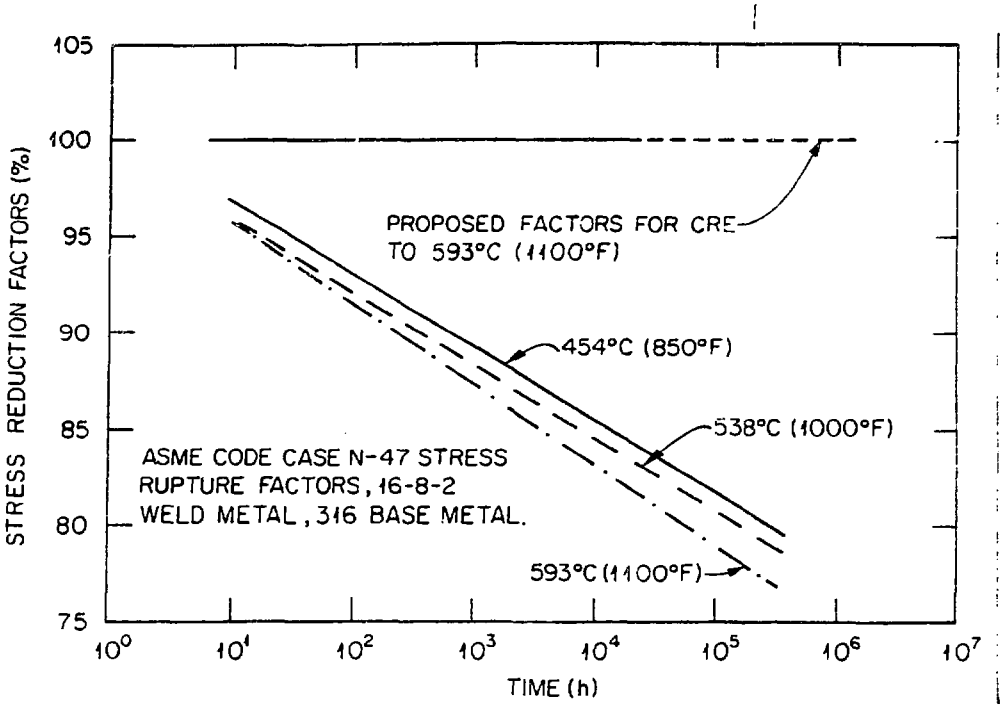

Fig. 26. Stress reduction factors according to ASME Code Case N-47 for 16-8-2 controlled residual element (CRE) and commercial 16-8-2 welds for temperatures to 593°C (1100°F). (Ref. 21).

CASTINGS

The mechanical behavior of castings of types 304 and 316 stainless steel, CF8 and CF8M, respectively has been investigated in the U.S. program. Castings of these two alloys have been used for core lower internal structures and for several components of sodium pumps. For some components, such as pump impellers, the use of castings is the only feasible method for producing complex geometries.

The mechanical properties of CF8 and CF8M are very sensitive to the δ-ferrite content and morphology in these materials.[22-24] The initial thermodynamic states and microstructures of these castings are extremely unstable when exposed to temperatures above about 350°C (662°F).[22-24] The δ-ferrite present in the original cast material has a very large influence on the mechanical properties of these materials for times to the design lifetimes of the power plants in which they are used. During service exposure to temperatures above 538°C (1000°F) the δ-ferrite transforms to sigma phase and austenite. At lower temperatures it transforms to austenite and alpha prime phase, which is a chromium-rich (~26% Cr) phase.[22-24] Both sigma and alpha prime phases reduce the ductility of CF8 and CF8M. The ferrite content and morphology present in the initial cast structure determine the distribution and geometry of the resulting sigma or alpha prime phases and austenite produced during elevated-temperature exposure. Recall

that formation of sigma phase results in large decreases in the toughness properties of austenitic stainless steels.[2] Sigma and alpha prime phases have a much larger detrimental effect on mechanical properties when they are acicular or form continuous or semicontinuous networks within the austenite than when they are present as isolated globules. High initial δ-ferrite contents (>15%) and very large δ-ferrite islands in the original cast structure result in mechanical properties that are inferior to those of castings with low (5–12%) initial δ-ferrite contents and small isolated δ-ferrite islands.

To avoid the uncontrolled transformation of δ-ferrite to sigma phase and austenite during power plant operation, most castings are given a dimensionally stabilizing heat treatment before use at elevated temperatures. The heat treatments are called dimensionally stabilizing because the transformation from the less dense δ-ferrite to sigma phase and denser (close-packed structure) austenite densifies the casting. This densification results in dimensional changes in the casting. The magnitude of the dimensional decrease of the casting is proportional to the initial δ-ferrite content of the casting and the amount of stress relaxation that occurs during the heat treatment.

Determination of the effects of initial δ-ferrite content and morphology on the mechanical properties of CF8 and CF8M for applications in LMFBR components is a high-priority task within the current U.S. LMFBR Materials and Structures Program. Measurements are in progress to determine the effects of long-term [10^4 to 5×10^4 h (about 1 to 6 years)] aging and of dimensionally stabilizing heat treatments on the tensile, creep-rupture, fatigue, and fracture mechanics properties of CF8 and CF8M.

Figure 27 shows the microstructure and microhardness indention marks in CF8M with a δ-ferrite content of 20 to 25% (*a*) in the as cast condition, (*b*) after 168 h at 482°C (900°F), and (*c*) after 24 h at 732°C (1350°F). In Fig. 27(*a*) the austenite appears white and the δ-ferrite appears gray. Note the small difference in hardness between the austenite and ferrite as shown by the size of the hardness indentation. Figure 27(*b*) shows very large increase (77%) in the hardness of the ferrite, with no observable change in its microstructure; the structure and hardness of the austenite remain approximately constant. Figure 27(*c*) shows an observable change in the microstructure of the ferrite, and its hardness is a little less than that shown in (*b*); again the structure and hardness of the austenite exhibit little change.

The room-temperature Charpy impact properties of this material were measured in the as-cast condition and after the dimensionally stabilizing heat treatment given the material shown in Fig. 27(*c*). Table I contains the Charpy impact values for these two conditions. The dimensionally stabilizing heat treatment results in a severe embrittlement of the casting with a decrease in the average Charpy impact energy from an 381 to 12 J (207 to 9 ft-lb). This is consistent with the 80% reduction in Charpy impact properties observed by Landerman and Bamford after aging of CF8M (ref. 22). Testing is under way to measure the effects of dimensionally stabilizing heat treatments on the other mechanical properties of CF8M.

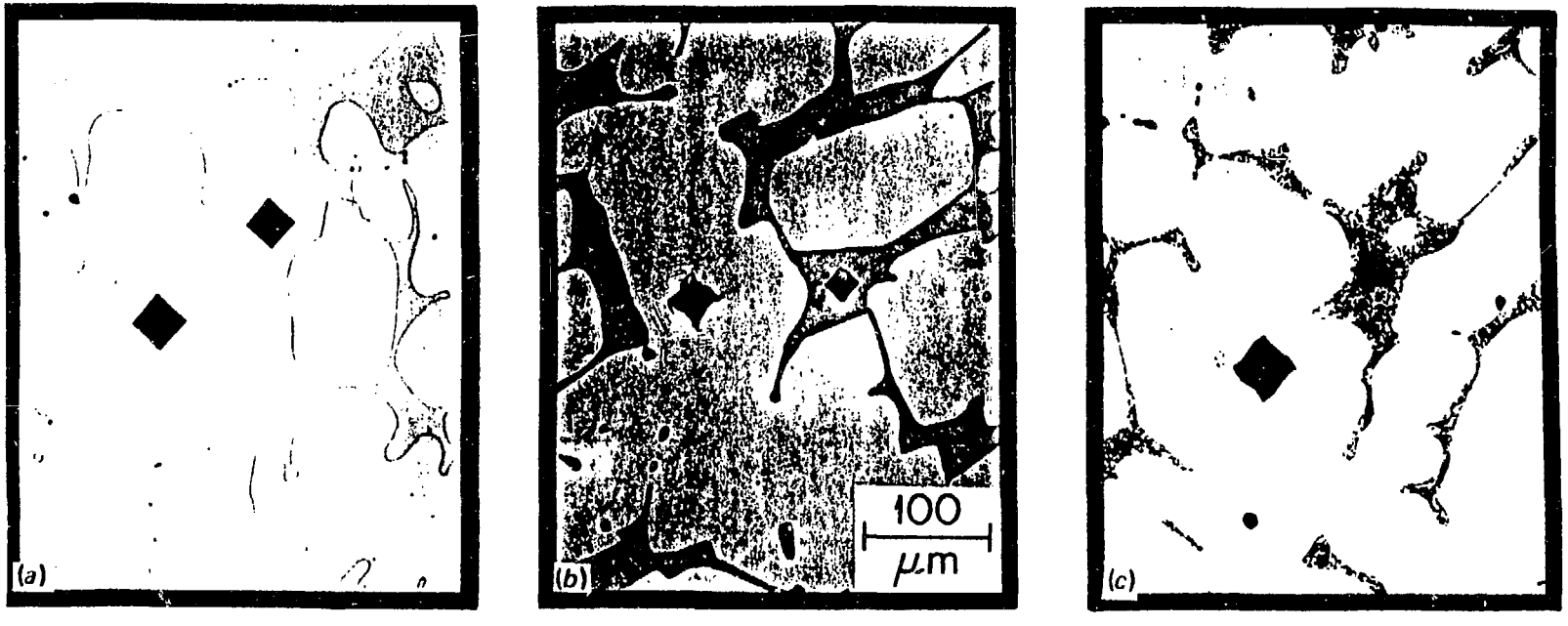

AS-CAST
γ = 185 ± 6 dph
α = 235 ± 22 dph

AS-CAST + 482°C for 168h
γ = 172 ± 4 dph
α = 417 ± 60 dph

AS-CAST + 732°C for 24h
γ = 163 ± 7 dph
α = 372 ± 98 dph

Fig. 27. Optical micrographs showing austenite, ω-ferrite, and microhardness indentions in CF8M. (*a*) As cast. (*b*) After 168 h at 482°C (900°F). (*c*) After 24 h at 732°C (1350°F).

SUMMARY

The information presented in this paper supports the following conclusions:

- The long-term mechanical properties of types 304 and 316 stainless steel can be correlated with the microstructures that are produced during elevated-temperature testing and/or service exposure relevant to LMFBR application.
- Long-term aging to 9.1 × 10^4 h (about 10 1/2 years) at temperatures to about 600°C (1100°F) has no detrimental effect on the tensile strength of type 316 stainless steel.
- Long-term aging to 9.1 × 10^4 h (about 10 1/2 years) at temperatures to about 600°C (1100°F) decreases the ductility of type 316 stainless steel; however, after 9.1 × 10^4 h at 649°C the ductility is still adequate for any anticipated out-of-core applications.
- Creep loading before tensile loading reduces the tensile properties of type 304 stainless steel.
- Fatigue loading before tensile loading has no effect on the tensile properties of type 304 stainless steel, but cyclic creep-fatigue loading reduces tensile ductility.
- For long-term testing and aging [~7 × 10^4 h (about 11 years)] of types 304 and 316 stainless steel, the stress-rupture properties exceed the minimum given in ASME Code Case 1-47.
- For type 316 stainless steel, the precipitate structure produced by aging before creep loading increases the steady-state creep rate and creep ductility and may slightly increase the time to rupture.
- The precipitate structures that form during long-term aging or service exposure at elevated temperature decrease the room-temperature Charpy impact values of type 316 stainless steel and its weldments with type 16-8-2 filler metal.
- Short-term (about 1 to 3 months) aging increases the fatigue life and creep-fatigue life of type 316 stainless steel by strengthening the grain boundaries.

Table I. Decrease in room-temperature Charpy impact energy due to heat treatment of CF8M

Charpy impact energy			
As cast		Heat treated at 732°C for 24 h	
(J)	(ft-lb)	(J)	(ft-lb)
Longitudinal			
261	192	8	6
277	204	9.5	7
267	195	12	9
Transverse			
245	180	15	11
268	197	11	8
272	200	18	13
Thickness			
326	240+	9.5	7
295	217	13.5	10
317	233	12	9

- Long-term aging to 1.25×10^5 h (about 14 1/2 years) produces $M_{23}(C,N)_6$, sigma phase, and δ-ferrite in types 304 and 316 stainless steel consistent with the time-temperature-precipitate diagrams of Weiss and Stickler;[2] therefore, the Weiss and Stickler diagrams may be used to predict long-term behavior of these alloys for LMFBR service.
- Combined addition of small controlled concentrations of boron, phosphorus, and titanium to produce a fine equiaxed microstructure provides a significant improvement to the creep-rupture properties of types 308, 316 and 16-8-2 welds.
- Transformation of δ-ferrite to austenite and sigma or alpha prime phases during aging or dimensionally stabilizing heat treatments can produce very large reductions in the room-temperature Charpy impact properties of CF8M cast stainless steel with initial δ-ferrite contents greater than 15%.
- The mechanical properties of types 304 and 316 stainless steel appear to be satisfactory for the temperature and load conditions anticipated for the design lifetimes of commercial LMFBR out-of-core structures and components.

ACKNOLWEDGMENTS

The authors wish to express their appreciation to R. W. Swindeman, M. L. Grossbeck, and Sigfred Peterson for reviewing this paper, to D. L. LeComte for preparation of the manuscript, and to Donna Amburn for preparing many of the figures.

REFERENCES

1. "World's Nuclear Reactors, No. 65 — Clinch River," *Nucl. Eng. Int.* 19, 843 (October 1974).

2. B. Weiss and R. Stickler, "Phase Instabilities During High Temperature Exposure of 316 Austenitic Stainless Steel," *Metall. Trans.* 3, 851–66 (April 1972).

3. C. R. Brinkman, V. K. Sikka, and R. T. King, "Mechanical Properties of Liquid-Metal Fast Breeder Reactor Primary Piping Materials," *Nucl. Technol.* 33, 76–97 (1977).

4. M. A. Cordovi et al., pp. 8–55 in *Behavior of Superheater Alloys in High Temperature, High Pressure Steam*, American Society of Mechanical Engineers, New York, 1968.

5. J. Hoke and F. Eberle, *Trans. ASME* 79, 307–17 (1957).

6. L. D. Blackburn, Hanford Engineering Development Laboratory, private communication to V. K. Sikka, 1975.

7. J. M. Steichen, HEDL-TME 75-15, Hanford Engineering Development Laboratory, Richland, Wash., January 1975.

8. D. Fahr, ORNL/TM4292, Oak Ridge National Laboratory, Oak Ridge, Tenn., November 1973.

9. V. K. Sikka, C. R. Brinkman, and H. E. McCoy, Jr., "Effect of Thermal Aging on the Tensile and Creep Properties of Types 304 and 316 Stainless Steels," pp. 316–50 in *Structural Materials for Service at Elevated Temperatures in Nuclear Power Generation*, ed. A. O. Shaffer, MPC-1, The American Society of Mechanical Engineers, New York, 1975.

10. V. K. Sikka, "Elevated Temperature Ductility of Types 304 and 316 Stainless Steel," pp. 129–48 in *Ductility and Toughness Considerations in Elevated Temperature Service*, MPC-8, The American Society of Mechanical Engineers, New York, 1978.

11. V. K. Sikka and C. R. Brinkman, "Influence of Prior Creep Strain on the Short-Term Properties of Types 304 and 316 Stainless Steel," pp. 497–501 in *Proc. 2d Int. Conf. Mechanical Behavior of Materials*, American Society for Metals, Metals Park, Ohio, 1976.

12. R. W. Swindeman, V. K. Sikka, and R. L. Klueh, "Residual and Trace Element Effects on the High-Temperature Creep Strength of Austenitic Stainless Steels," *Metall. Trans. A* 14A, 581–93 (April 1983).

13. V. A. Biss and V. K. Sikka, *Metallographic Study of Type 304 Stainless Steel Long-Term Creep-Rupture Specimen*, ORNL/TM-7618, Oak Ridge National Laboratory, Oak Ridge, Tenn., January 1981.

14. R. Stickler and A. Vinckier, "Morphology of Grain-Boundary Carbides and Its Influence on Intergranular Corrosion of Type 304 Stainless Steel," *ASM Trans. Q.*, 54, 362–80 (1961).

15. C. F. Etinne, W. Dortland, and H. B. Zeedijk, "On the Capability of Austenitic Steel to Withstand Cyclic Deformation During Service at Elevated Temperature," pp. 225.1–9 in *Int. Conf. Creep Fatigue in Elevated Temperature Applications*, vol. 1, the Institution of Mechanical Engineers, London, 1975.

16. F. G. Wilson, "The Morphology of Grain and Twin Boundary Carbides in Austenitic Stainless Steels," *J. Iron Steel Inst. (London)* 209, 126–30 (1971).

17. C. E. Spaeder, Jr., and K. G. Brickner, pp. 143–50 in *Advances in the Technology of Stainless Steels and Related Alloys*, ASTM STP 369, American Society for Testing and Materials, Philadelphia, 1965.

18. D. P. Edmonds, R. T. King, and G. M. Goodwin, "Residual Elements Have Significant Effects on the Elevated-Temperature Properties of Austenitic Stainless Steel Welds," pp. 56–68 in *Properties of Austenitic Stainless Steels and Their Weld Metals (Influence of Slight Chemistry Variations)*, ASTM STP 679 American Society for Testing and Materials, Philadelphia, 1979.

19. D. P. Edmonds, D. M. Vandergriff, and R. J. Gray, "Effect of Delta Ferrite Content on the Mechanical Properties of E308-16 Stainless Steel Weld Metal. III. Supplemental Studies," pp. 47–61 in *Properties of Steel Weldments for Elevated Temperature Pressure Containment Applications*, ed. G. V. Smith, MPC-9, American Society of Mechanical Engineers, New York, 1978.

20. R. T. King, J. O. Stiegler, and G. M. Goodwin, "Relation Between Mechanical Properties and Microstructure in CRE Type 308 Weldments," *Weld. J. (Miami)* 53, 307–13-S (1974).

21. G. M. Goodwin, ORNL, personal communication, July 1983.

22. E. I. Landerman and W. H. Bamford, "Fracture Toughness and Fatigue Characteristics of Centrifugally Cast Type 316 Stainless Steel Pipe After Simulated Thermal Service Conditions," pp. 99–128 in *Ductility and Toughness Considerations in Elevated Temperature Service*, MPC-8, American Society of Mechanical Engineers, New York, December 1978.

23. M. P. Malone, "Sigma and 885°F Embrittlement of Chromium-Nickel Stainless Steel Weld Metals," *Weld. J. (N.Y.)* 46, 241–53-s (1967).

24. A. Trautwein and W. Gysel, "Influence of Long-Time Aging of CF8 and CF8M Cast Steel at Temperatures Between 300 and 500°C on Impact Toughness and Structural Properties," pp. 165–89 in *Stainless Steel Castings*, ed. V. G. Behal and A. S. Melilli, ASTM STP 756, American Society of Testing and Materials, Philadelphia, 1982.

DISCLAIMER